The Dynamics of Alliance and Hostility in Social Structures

Seán Ernest Murray

supervised by
Prof. A Goriely & Prof. R Lambiotte

Oriel College
September, 2021

A dissertation submitted for partial fulfilment of the degree MSc in Mathematical Modelling and Scientific Computing

Acknowledgements

First and foremost, I'd like to thank my supervisors, Prof. Goriely and Prof. Lambiotte, who selected me to pursue this dissertation, and whose guidance and encouragement helped me to follow a course through the work in which I had a keen interest. I thoroughly enjoyed working with both of you.

I'd like to thank the MMSC cohort, who were always fun to be around and willing to help one another when the going got tough.

A sincere thank you to the teaching assistants of the core courses, especially Matthew Hennessy and Ciaran Crawford.

I'd also like to acknowledge the special group of people I lived with in SC34, including Erik, with whom early discussions helped me find my feet in this dissertation.

A thank you to a long-term friend, James Noonan, without whom I might never have discovered this course.

I'm deeply grateful for my parents, John and Finuala, for supporting me on my Oxford journey.

A final word of thank you to the course director, Dr Kathryn Gillow, who is always on your side. Her dedication and commitment to the programme is inspiring and was deeply appreciated this year, by myself and by everyone in the cohort.

Abstract

This dissertation explores the formation of social structures on signed graphs from the perspective of dynamical systems. We outline what it means for a graph of relations to be balanced, motivated by concepts in social psychology. We investigate and compare existing models of opinion dynamics through gossiping mechanisms, and explore how they affect the structure of social groups. Such dynamics tend to diverge, hence we investigate known models that bound the opinions to a prescribed range. We then present new convergence proofs and prove the stability of different social states under such models.

We outline a novel control model, which nudges the opinions towards a social configuration prescribed by a state vector, termed the diplomatic target. We apply this model to two case studies: the alliances and enmity of nations in the period preceding WWI; and *Zachary's karate club study*, a well-known example of group fission in network theory. Our model correctly classifies the final allegiances in both cases. We also introduce and investigate the bifurcating dynamics on two coupled graphs, known as a multiplex graph, and prove the stability of various fixed points of the associated system. We find that coupled graphs can tend toward separate states of balance and still be stable under the presented dynamics, interpreting this in the context of social networks.

Contents

List of Figures

Chapter 1

Introduction

How might we model the dynamics of friendship and enmity? In this dissertation, we investigate the social structures which emerge from continuous-time dynamic models, and their associated stability, control, and application to more complex graph topologies. The key concept underpinning such models is that of the signed opinion graph, where signed edges quantify the strength of positive or negative relations between vertices representing social entities, encoded in the associated entries of a signed matrix X. The dynamics are represented as initial value problems in X, which in their basic form consist of simple matrix operations representing a gossiping mechanism, each vertex updating its opinion of another by considering all of the relative opinions in the graph.

The relation between three simply connected entities, known as a triad, is considered socially balanced if there is an odd number of positive opinions between them. In a fully connected graph, a necessary and sufficient condition for the entire graph to be socially balanced is if all of the constituent triads are balanced [1]. In such a case, the graph can be partitioned into two feuding factions: mutually exclusive cliques within which relations are positive, and between which relations are negative.

The overall aims of this dissertation are: to analyse how opinion dynamics drive initially imbalanced graphs to balanced states, along with their associated stability and convergence criteria; to present and test control mechanisms to drive graphs to a desired state; and to generalise the dynamics to more complex multiplex graph topologies.

Throughout the work we seek to interpret our mathematical analysis through the lens of social relations: graph edges represent opinions; dynamics represent the effects of communication and gossiping; control represents biases, historical allegiances, or known opinion influences; and layers of multiplex graphs represent different arenas of social interaction between the same entities.

The layout of the dissertation is as follows. In Chapter 2 we introduce the socio-psychological basis and subsequent graph-theoretic formulation of social balance theory. We outline the theorems and associated proofs which ground the intuition behind the 'balancing effect' of dynamical models of opinion networks and motivate the use of models in continuous time. We then explore existing continuous-time models in Chapter 3, their associated conditions for bringing an initial random graph to a state of balance, and how the dynamics may be bounded to prevent opinions diverging. We consider an alternative model on directed graphs. Chapter 4 contains the bulk of the novel contributions of the dissertation. We outline proofs of convergence and the stability of balanced states for a non-diverging model. We present a control mechanism that leads the graph to a desired state, termed the diplomatic target. Two cases are presented, applying the model to international relations preceding WWI and to a study of social fission of members in a karate club. We then generalise the bounded dynamics to multiplex graphs, and analyse the associated convergence and stability of balanced states. We outline natural extensions to the work and conclude in Chapter 5.

Chapter 2

Background

In complex systems science, there are three broad approaches used to model friendship, enmity, and conflict.

The first concerns statistical modelling, which dates back to the 1940s where Richardson [2] showed that the distribution of fatalities of conflicts follow power laws. Examples of more modern approaches include data-mining of news sources to gauge political sentiment [3], or modelling incidents of acts of terror as self-exciting Hawkes processes, such as those during the Troubles [4]. Cervantes [5] used a decision-tree algorithm to predict conflict between nations based on data such as flights, migration, and visa requirements. These approaches are powerful, but data-constrained, and lack the deeper understanding of dynamic mechanisms at play, the models sometimes lacking explainability or providing any causal inference.

Another approach is via agent-based modelling (ABM), involving the simulation of a large number of interacting agents following simple instructions, allowing us to investigate claims and causal mechanisms such as the distribution of political responsibility, gang rivalry [6], ethnic and culturally-motivated differentiation and violence [7], and the role of warfare in the emergence of large societies [8]. The main drawback of ABM however is that it is limited by complexity for which, in large-scale systems, the associated algorithms quickly become intractable.

The final approach is in dynamic modelling of interactions. Dynamical models of the relations between entities in a network may be prescribed by the rules of social balance, spatial distribution, or other indicators such as military imbalances and well-being metrics [9]. This is the general approach taken in this disserta-

tion, as it is interesting mathematically and does not rely on a replete dataset, computational tractability, data-model fits, or much of the work involved in data mining.

This chapter outlines requisite knowledge from network theory, details Heider's theory of social balance and its interpretation in the context of a signed graph, and motivates the dynamical models of opinion formation within such graphs.

2.1 Definitions from graph theory

We outline some background notions from network theory that are used in the course of the dissertation. Many of the definitions are available in Newman [10].

A *linear graph* represents pairwise relations between $n \in \mathbb{N}$ members or agents, denoted by $G(V, E)$ where V is a finite set of *vertices* or *nodes* $V = \{1, \ldots, n\}$ and $E = \{(i, j) | i, j \in V\}$ a prescribed list of (possibly ordered) pairs of vertices representing *edges*. Neighbouring vertices i and j are incident to the edge (i, j). The cardinality of V is the graph size, $|V| = n$. Computationally, edge lists are stored for representing a graph structure, but another useful means for representation is via an adjacency matrix $A \in \{0, 1\}^{n \times n}$, whose entries are given by,

$$A_{ij} = \begin{cases} 1, \text{ if } (i, j) \in E \\ 0, \text{ otherwise.} \end{cases}$$

Entries A_{ii} represent *self-loops* or reflexive relationships. The presence or absence of such relations is acknowledged in different models presented in the course of this dissertation. Inclusion of a negative relation, such that $A \in \{-1, 0, 1\}^{n \times n}$, constitutes a *signed graph*.

In *directed graphs*, the orientation of an edge between two vertices is specified in the order by which the pair is given in E, (i, j) indicating an edge from i to j. Correspondingly, adjacency matrices of directed graphs are typically asymmetric. Traditionally the A_{ij} entry represents an edge *from j to i* [10], yet much of the literature relevant to this dissertation specifies the A_{ij} entry as an edge *from i to j*, hence we follow the latter convention.

In regular linear graphs, edges are treated as a binary specification of the relation between two vertices. To allow for a varying strength of relations, *weighted*

graphs are used. In a weighted graph, $G(V, w)$, a function w generally quantifies a non-negative edge-weight between two vertices. In this dissertation, however, we are concerned with weights that vary over the entire real line, $w : V \times V \to \mathbb{R}$ instantiating $G(V, w)$ as a *signed weighted graph*. The idea is that the inclusion of negative weights allows for the specification of both positive and negative social relations between vertices representing social entities. In the case where w is symmetric,

$$w(i, j) = w(j, i), \quad \forall\, i, j \in V,$$

and G is undirected. The signed weighted adjacency matrix is denoted as $X \in \mathbb{R}^{n\times n}$, with entries

$$X_{ij} = w(i, j).$$

A sequence of $v_1, \ldots, v_p, v_{p+1}$ neighbouring vertices is known as a *path* of length p. In the case where $v_1 = v_{p+1}$ the path is a *cycle*. The vertices comprising a cycle of length three form a *triad*. In a signed graph, the *sign of a cycle* is the product of the signs of the vertices that make up the cycle.

The *degree* of a vertex is the number of edges incident to that vertex. The graph G is considered *fully connected* or *complete* when every vertex is connected to every other vertex in G. In the case where $w(i, j) = 0$ for many pairs of vertices, i.e. $|E| \ll |V|$, the graph and adjacency matrix X are considered *sparse*. An example of such is a triangular lattice graph with large $|V|$ where, in the case of periodic boundary conditions, every vertex has degree 6, independent of $|V|$, which we refer to in later sections.

Multiplex graphs are representations of multilayer networks where the node-set V is identical across each layer [11]. In cases where the node-set across each network is different, the graph is referred to as *multilayer* [5]. For a multiplex network with n vertices in each $l = 1, \ldots, L$ layers, the associated adjacency matrix for a given layer $l \in L$ is given by $X_{(l)} \in \mathbb{R}^{n\times n}$. The parentheses are omitted in cases where the meaning is unambiguous.

When representing social networks, a number of notions relating to the structure and dynamics of signed graphs may be defined, chiefly the notions of balanced relations and balanced graphs. To motivate these, we first outline some of the underlying socio-psychological concepts of Heider and the gap to graph theory that

was bridged by Harary and Cartwright [1]. Beyond social systems, notions of balance and frustration are observed in Ising's model of magnetic spin-glasses [12].

2.2 Heider's Theory of Social Balance

The notions of social balance date back to Heider's theory of attitudes and cognitive organisation in social systems [13]. Here, the balance of subjective social relations between entities is considered based on 'attitudes' L, i.e. liking and disliking, and 'cognitive units' U such as possession, belonging, and proximity. A balanced state is defined between two entities if the relation between them is positive or negative with respect to all meanings of L and U. In a set of three entities, also known as a triad, a balanced state exists when all relations are positive, or two are negative and one is positive. Heider's concept of relations tending towards such balanced states is driven most typically by communication between entities.

Newcomb [14] develops a more objective theory (in the sense of not stating internal states of entities) based on interpersonal communication, where the relations between entities may be inferred based on how they exchange information. Newcomb's notion of relations which "strain towards symmetry" is applied to studies on attraction and group homophily, concluding that entities will continue or discontinue their association to increase attraction and perceived symmetry, reflecting Heider's more general theory of "tendency towards balance".

The common denominator of both theories is that communication between entities is the mechanism by which social groups move towards states of balance. This is the idea we keep in mind when investigating various dynamical models.

2.3 Harary-Cartwright formulation

Cartwright and Harary propose a generalisation of Heider's social balance from a graph-theoretic perspective [1]. Given that the sign of a cycle or path is the product of the signs of the constituent edges, a cycle with a positive sign is considered *balanced*. This leads to the following theorem by Harary-Cartwright defining a *balanced graph*, the proofs for which are outlined in [15].

Theorem 1. *A signed graph G is balanced if and only if the sign of every cycle in G is positive.*

An equivalent definition relating to the sign of any given path between two points is given by the following theorem.

Theorem 2. *A signed graph is balanced if and only if every path between each pair of distinct vertices has the same sign.*

From a computational perspective, Theorem 2 is not very interesting, as the cost of checking the sign of every path between every distinct pair of vertices, $\mathcal{O}(n^3)$ [16], is equivalent to checking the balance of every cycle in the graph as per Theorem 1. What is more relevant is the interpretation of how influence is exerted between entities in a balanced graph G. If we consider the sign of an edge denoting a positive or negative influence, the influence of vertex A on vertex B will be the same no matter what path in G the influence passes from A to B.

Some imbalanced graphs may be closer to balance than others. The coherence of influence exerted on an individual is thus a function of how close the graph is to balance. This is quantified via the *degree of balance* of a graph, defined as the ratio of positive cycles to total cycles. If $C(G)$ and $C^+(G)$ are the number of cycles and positive cycles, respectively, the degree of balance of G is

$$b(G) = \frac{C^+(G)}{C(G)}.$$

Note that $b(G)$ depends on the structure of the graph, and can only take discrete values. For instance, a graph consisting of a single imbalanced triad has $b(G) = 0$. Hence, as advised by Harary-Cartwright, any interpretation of a specific value $b(G)$ should account for the distribution of $b(G)$, determined by the structure of G.

A balanced graph exhibits an interesting property where it may be partitioned into two mutually exclusive consortia or *factions*, where relations are positive within factions and negative between factions. The Structure Theorem [15] formalises this notion, which is also referred to as social mitosis [17]. Note that one faction may have size zero, in which case the entire graph is in a state of *consensus* or 'utopia', otherwise the state is termed *bipolar*.

Theorem 3 (Structure Theorem)**.** *A fully connected signed graph, G, is balanced if and only if its vertices can be partitioned into two cliques, V_1 and V_2, within each all edges are positive and between each all edges are negative.*

Proof.

Necessity. Let A_1 be any vertex of G, where V_1 is the set of A_1 and all vertices positively adjacent to A_1, and V_2 the set of vertices negatively adjacent to A_1. Then $V_1 \cap V_2 = \varnothing$. In V_1, any two distinct points B_1 and C_1 are positively adjacent. If either B_1 or C_1 are A_1 then this is true by construction, otherwise the cycle $A_1B_1C_1$ contains positive edges A_1B_1 and A_1C_1. For a balanced graph this cycle is balanced, hence B_1C_1 must also be positive. For vertices $B_2 \in V_2$, $C_2 \in V_2$ the edge B_2C_2 must be positive for the cycle $A_1B_2C_2$ to be positive, similarly for $B_1 \in V_1$, $C_2 \in V_2$, the edge A_1B_1 must be positive for $A_1B_1C_2$ to be positive.

Sufficiency. Assuming the graph may be arranged into two opposing cliques as stated in the theorem, every cycle in G contains an even number of negative edges between cliques V_1 and V_2. Hence every cycle in G is positive and by definition G is balanced. □

The proof of necessity relies on the fact that triads (cycles of length three) are balanced if they contain two or zero negative edges.

A result of the structure theorem is that the associated adjacency matrix of a balanced graph will have some permutation of the following block sign structure,

$$X = \begin{pmatrix} + & \\ & + \end{pmatrix} \text{ or } \begin{pmatrix} + & - \\ - & + \end{pmatrix} \in \mathbb{R}^{n \times n}$$

The sign structure of X may be easily permuted and displayed to check if the above sign structure holds. From a computational perspective, this is useful in our context as a visual confirmation of social balance.

The Structure Theorem may be interpreted from a perspective of influence exertion. Given two cliques obeying the structure theorem (thus instantiating a balanced graph), we find the exertion of influence will "produce homogeneity within cliques and opposing opinions between cliques", creating diverging opinion magnitudes i.e. polarisation. As noted, the exertion of influence becomes more coherent or, in Heider's terms, the tendency towards balance becomes more pronounced, as

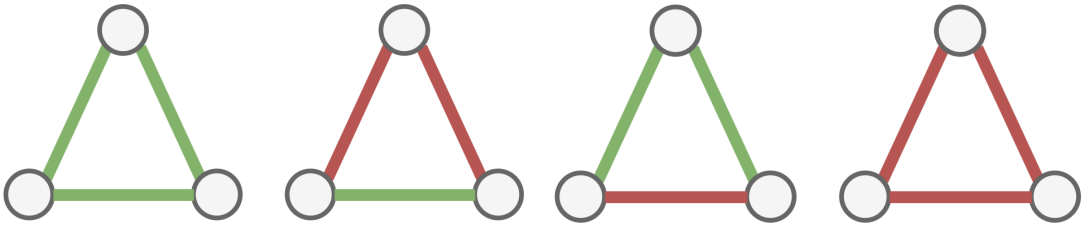

Figure 2.1: *"My enemy's enemy is my friend"* [1]. Balanced (left, mid-left) and imbalanced (right, mid-right) triads.

the graph approaches a balanced state. This also reflects the *echo hypothesis* [18], where opinions within a balanced group, either positive or negative, are enhanced by further communication with others. Furthermore, this argument can also be made via *homophily* [10] - as two factions emerge there is a stronger, not weaker, social pressure to *conform with one faction or another*.

The analytic effect of increasing influence exertion is witnessed in dynamical models where edge-weights and time are continuous [17, 19, 20]. In these cases, positive and negative edge-weights diverge as the graph tends towards a balanced state. This is one of the reasons motivating our focus on continuous models.

2.4 Social balance and triadic relations

In complete graphs, a sufficient condition for a complete graph to be balanced is if all of the triads $\triangle_{ijk}$ in the graph are balanced [21],

$$X_{ij}X_{ik}X_{jk} > 0, \quad \forall\, i, j, k \in V.$$

The central idea is that "friends agree in their opinion of a third party". In social systems, there is typically an overexpression of the balanced triads shown in Figure 2.1 [5]. It has been shown that social entities which are part of an imbalanced triad experience stress, also termed social frustration or cognitive dissonance, and tend to change their opinions to reduce the number of imbalanced triads in their social network [22]. Hence, this naturally motivates the investigation of dynamical models which drive a graph towards a socially balanced state.

2.5 Social balance and conflict

Explicit prediction of conflict is notoriously difficult versus other events such as earthquakes as, by definition, social actors involved in the outbreak of conflict break rules. The essay [23] provides an overview on the challenges of such prediction. However, in practice social entities are observed to arrange themselves into a balanced configuration before the outbreak of widespread bilateral conflict, indicating that standard social balance and the threat of large-scale conflict are positively correlated. A noteworthy example of this is the diplomatic relations between entities leading up to WWI. The alliances and defections between nations in the years preceding WWI are illustrated in Figure 2.2, as detailed by Antal *et al.* [24]. As is shown, the final state may be partitioned into two mutually opposing factions, in this case representing the Axis and Allied forces which, by the Structure Theorem, constitutes a socially balanced graph. This is merely noted as an empirical example in Antal *et al.*, however, we present a comparison and verification with our own models in later sections.

The literature is replete with other examples of the connection between social organisation, conflict, and Heider's balance theory. Moore [25] presents five studies of international conflicts which result in perfect or near-perfect balance. Cervantes [5] studies multilayer networks of nations, deriving a multilayer balance measure that was shown to have a high correlation with the subsequent outbreak of conflict. Smeets *et al.* [26] analyse 170 present-day Dutch novels, finding that the "majority of triadic conflicts exist in a state of social balance". Szell *et al.* [27] study six different types of interaction between agents in a massive online multiplayer game, providing a multiplex network validation of structural balance theory. Numerous other examples are referenced in the survey article [21].

2.6 Discrete dynamics

Antal *et al.* [24] present discrete-time and weight models of dynamics of triads in a fully connected graph, such that $A \in \{-1, 1\}^{n \times n}$. They investigate the long-time dynamics and phase transitions with respect to the density of friendly edges, ρ, in the graph. The idea is that the models reflect known human behaviour to

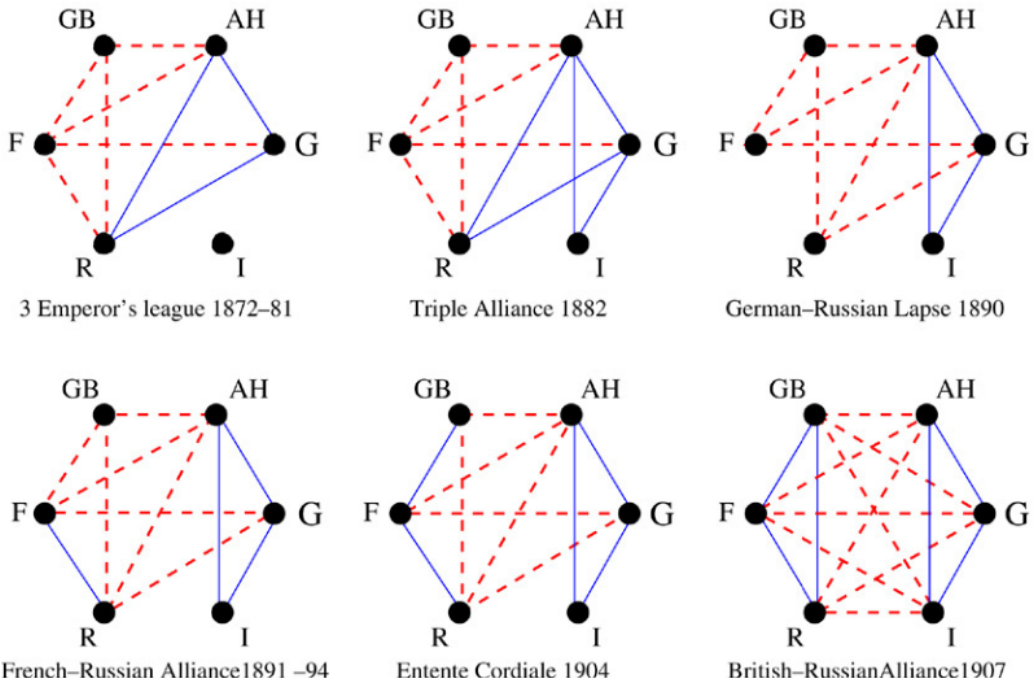

Figure 2.2: Faction formation in the period 1872-1907 prior to the outbreak of World War I in 1914, from [24]. Blue lines indicate alliance, dashed red lines indicate enmity. Countries listed are Great Britain (GB), Austria-Hungary (AH), Germany (G), Italy (I), Russia (R), and France (F).

reduce the number of imbalanced triads in a social environment. Two models are presented: local triad dynamics (LTD) and constrained triad dynamics (CTD).

The social interpretation of LTD is of the "social graces of the clueless", where friends are formed randomly without consideration of how the balance of other relationships is affected. The governing model consists of a master equation containing four compartments, describing the stochastic change in densities of triads with $k \in \{0, 1, 2, 3\}$ unfriendly links.

In CTD, a random relationship is flipped provided it increases the total number of balanced triads. This may be interpreted as the dynamics of a graph consisting of individuals who, when changing a relationship, will first consider the balance of their entire social network.

A number of criticisms may be levelled against discrete approaches versus continuous ones. First is the lack of agreement between qualitative arguments and numerical results which are outlined for CTD in [24]. Additionally, graphs following discrete models are shown to approach a balanced state asymptotically. This contradicts the notions of influence exertion introduced earlier[1], a limitation not witnessed in continuous models. Furthermore, the decision of 'which link to flip' is not encountered in continuous models. Finally, discrete dynamics such as LTD contain fixed points at imbalanced graph states, known as *jammed states*. Such phenomena are not typically encountered in continuous dynamical models, which hence motivate the focus on the latter from here onward.

[1] As the graph tends towards balance, the exertion of influence is more coherent, hence the rate at which the graph tends towards balance becomes greater.

Chapter 3

Continuous dynamics

This section investigates various models available in the literature for the generic matrix initial value problem, with $X(t) \in \mathbb{R}^{n\times n}$,

$$\dot{X} = F(X), \quad X(0) = X_0. \tag{3.1}$$

Kułakowski *et al.* [17] first introduce a dynamical model of social balance in which $X(t) \in \mathbb{R}^{n\times n}$ represents the weights of an adjacency matrix of a graph G, which are allowed to vary continuously in time. This approach is taken to allow edges to vary in strength as well as in sign. $X(t)$ is interpreted as an opinion or reputation matrix, where the entry X_{ij} denotes vertex i's opinion of vertex j, positive (negative) entries indicating friendly (hostile) relations. The differential equation (4.1) specifies how the opinions of each vertex are updated. G is assumed to be a signed undirected graph, hence opinions between nodes are symmetric, $X(t) = X(t)^T$, $\forall\, t > 0$. As mentioned previously, the triad $\triangle_{ijk}$ composed of vertices i, j, k, is balanced if $X_{ij}X_{ik}X_{kj} > 0$.

For symmetric initial conditions, the following continuous-time model is proposed in [17],

$$\dot{X} = X^2, \quad X(0) = X(0)^T, \tag{3.2}$$

or, in elementwise notation,

$$\dot{X}_{ij} = \sum_{k\in V} X_{ik}X_{kj}, \quad i, j \in V. \tag{3.3}$$

We may interpret this matrix differential equation as a *gossiping mechanism*. Here i changes its opinion of j by considering the relative opinions of every vertex k.

This model reflects both Heider and Newcomb's theories in that communication is the mechanism of change in social structures. The product of the signs of edges X_{ik} and X_{kj} force X_{ij} in a direction that balances the triad $\triangle_{ijk}$. A variant of these dynamics excluding self-loops is shown to lead to a balance for $n = 3$ vertices [17]. Numerical results indicate balance is achieved for any n, however, this is not proven analytically.

Although the signs of the opinion matrix $X(t)$ reach a balanced state, the entries tend to blow up in finite time. This reflects the property mentioned earlier that graphs reaching balance are characterised by diverging opinions, where coherent influence exertion creates positive feedback. Yet, as argued in [17], extreme opinions tend not to spread as we prefer to be considered civilised. Additionally, the well-known Bogardus scale [28] quantifying social distance is finite. Thus to avoid the blow-up of opinions, an elementwise envelope function $C(X; R)$ is adopted based on Bogardus' social distance. This leads to the following non-linear, elementwise modification of the system

$$\dot{X}_{ij} = C(X_{ij}; R) \sum_{k \in V \setminus \{i,j\}} X_{ik} X_{kj} = \left(1 - \frac{X_{ij}^2}{R^2}\right) \sum_{k \in V \setminus \{i,j\}} X_{ik} X_{kj}. \tag{3.4}$$

where $R > 0$. Note that this introduces $n^2/2$ fixed points into the system satisfying $X_{ij} = \pm R \; \forall \, i, j \in V$, the factor of $1/2$ owing to X being symmetric. It is argued in [17] based on computational results that values of $R \geq 5$ do not influence the dynamics until balance is reached. For $R = \infty$, corresponding to $C(X; R) = 1$, the uninhibited system (3.2) is recovered. Note that in order to prove convergence to a balanced state and to analyse the stability of the fixed points in [17] and [29], the model (3.4) does not contain self-loops, i.e. $k \notin \{i, j\}$. We prove similar results for a model with self-loops in later sections.

The initial condition X_0 is chosen in [17] such that the upper triangular entries are independent and identically distributed (iid) random variables, drawn from a uniform distribution of unit width around zero, $X_{ij}(0) \overset{iid}{\sim} U(-1/2, 1/2)$, $i \leq j$. The strictly lower diagonal entries are then filled such that the matrix is symmetric.

Numerical results in [17] show that, given a large number of vertices $n > 100$, the time taken for the graph to reach a balanced state, t^*, follows

$$t^* \propto n^{-1/2}. \tag{3.5}$$

The authors justify this as (i) the velocity of an opinion or edge, $\dot{X}_{ij}$, is given as a summation over n nodes k in (3.2), which grows linearly in n, however (ii) in the initial condition $X(0) \sim U(-1/2, 1/2)$, the deviation of the sum of entries from zero decreases with $n^{-1/2}$. The total contribution of increasing n on the velocity is $n^{1/2}$, with time as its inverse hence given by (3.5). It is noted that this holds only when the initial distribution U is symmetric about zero.

3.1 Convergence to a balanced state

An open problem left in [17] is a proof for generic n that the system (3.2) will bring an initial symmetric matrix $X(0)$ to a balanced state. Marvel *et al.* [19] prove this for large n by developing a closed-form expression for faction membership as a function of the initial conditions, taking advantage of the symmetry of the problem via spectral methods. They show analytically that the signs of the graph edges converge to a balanced configuration consisting of either a bipolar or consensus state. The solution is shown to take the form $X(t) = Q\Lambda(t)Q^T$, where the eigenvectors remain constant with respect to time. It is also stated that this form of solution occurs more generally for $\dot{X} = F(X)$ when $F(X)$ is a polynomial. This is not proven in the paper, thus we derive it below.

Given a matrix polynomial of degree M, we let $F(X) = \sum_{m=0}^{M} a_m X^m$. The following proof shows that, assuming symmetric initial conditions, the solution takes the form $X(t) = Q\Lambda(t)Q^T$. Hence, it is sufficient to model the evolution of the eigenvalues $\Lambda(t)$ to understand the evolution of the whole system.

Letting $(\lambda_1, \lambda_2, \ldots, \lambda_n)$ denote the decreasing eigenvalues of $X(0)$, we express the initial conditions via a symmetric eigenvalue decomposition as

$$X(0) = Q\Lambda(0)Q^T, \quad \Lambda(0) = \operatorname{diag}(\lambda_1, \ldots, \lambda_n), \tag{3.6}$$

and letting $Y(t) = Q\Lambda(t)Q^T$, we show that $Y(t)$ is identical to the solution $X(t)$ by uniqueness. We differentiate $Y(t)$ with respect to time,

$$\dot{Y} = Q\dot{\Lambda}Q^T = QF(\Lambda)Q^T \tag{3.7}$$

and, as $QQ^T = I_n$, note that the polynomial in $Y(t)$ may be expressed as,

$$\begin{aligned} F(Y) &= \sum_{m=0}^{M} a_m Y^m \\ &= \sum_{m=0}^{M} a_m (Q\Lambda Q^T)^m \\ &= Q\left[\sum_{m=0}^{M} a_m \Lambda^m\right] Q^T \\ &= QF(\Lambda)Q^T. \end{aligned} \tag{3.8}$$

$Y(t)$ satisfies the flow $\dot{Y} = F(Y)$ and shares the initial condition $Y(0) = X(0)$, hence by uniqueness, $X(t) \equiv Y(t) = Q\Lambda(t)Q^T$. Given eigenvectors Q of $X(0)$, for a solution at time t it hence suffices to solve the eigenvalue evolution for $\Lambda(t)$,

$$\dot{\Lambda} = F(\Lambda), \quad \Lambda(0) = \mathrm{diag}(\lambda_1, \ldots, \lambda_n). \tag{3.9}$$

Now returning to the derivation outlined in [19] for $F(\Lambda) = \Lambda^2$, the solution to this decoupled (diagonal) system is

$$\Lambda(t) = \begin{pmatrix} \frac{\lambda_1}{1-\lambda_1 t} & & \\ & \ddots & \\ & & \frac{\lambda_n}{1-\lambda_n t} \end{pmatrix}, \quad t \geq 0. \tag{3.10}$$

Note that this solution is only valid when t is less than the minimum radius of convergence which, assuming the largest eigenvalue of $X(0)$ is positive, is given by $t < 1/\lambda_1$. The solution at a given time $X(t)$ may be expressed as a linear combination of rank-one matrices corresponding to the eigenvectors $Q = (\mathbf{q}_1, \ldots, \mathbf{q}_n)$, again for $\lambda_1 > 0$,

$$X(t) = \sum_{i=1}^{n} \Lambda_{ii}(t)\mathbf{q}_i\mathbf{q}_i^T, \quad t < \frac{1}{\lambda_1}. \tag{3.11}$$

Expanding denominators of Λ_{ii} in powers of t gives $X(t) = X(0) + X(0)^2 t + X(0)^3 t^2 + \ldots$ with which the solution may also be written

$$X(t) = X(0)\left[I - X(0)t\right]^{-1}, \quad t < \frac{1}{\lambda_1}. \tag{3.12}$$

Noting that the singularity occurs at $t_* = 1/\lambda_1$ given the conditions: (i) $\lambda_1 > 0$; (ii) $\lambda_1 > \lambda_2$; and (iii) all components of $\mathbf{q}_1$ are non-zero; we can see directly from the summation (3.11) that $X(t)$ collapses to the rank-one matrix,

$$\lim_{t \to t^*} X(t) = \Lambda_{11} \mathbf{q}_1 \mathbf{q}_1^T. \tag{3.13}$$

Normalising $X(t)$ by the Frobenius norm serves to remove the scaling term Λ_{11},

$$\lim_{t \to t^*} \frac{X(t)}{||X(t)||_F} = Q \, \mathrm{diag}(1, 0, \ldots, 0) \, Q^T = \mathbf{q}_1 \mathbf{q}_1^T. \tag{3.14}$$

3.1.1 Convergence conditions

There are three conditions for an initial symmetric random matrix (with entries drawn independently from a symmetric continuous distribution) to converge to a balanced state: (i) $\lambda_1 > 0$; (ii) $\lambda_1 > \lambda_2$; and (iii) all components of $\mathbf{q}_1$ are non-zero. All three are satisfied in the large-n limit, which is proven below, from [19].

(i) This requires more specification on the entries of $X(0)$. Given a symmetric probability distribution G the diagonal and off-diagonal entries are given by

$$\begin{aligned} X_{ij}(0) &\overset{iid}{\sim} G(\tau, \nu^2), \quad i < j \\ X_{ii}(0) &\overset{iid}{\sim} G(\mu, \sigma^2) \\ X_{ij}(0) &= X_{ji}(0), \qquad i > j. \end{aligned} \tag{3.15}$$

Given the second moments ν^2 and σ^2 of G are finite, it can be shown [30] that Wigner's semicircle law applies as $n \to \infty$ with high probability, which specifies that the distribution of the eigenvalues of $X(0)/\sqrt{n}$ is compact and centred around zero. Hence, in probability for large n, $\lambda_1 > 0$.

Note that in this dissertation we typically let the first and second moments be the same for all entries, $\tau = \mu$, $\nu^2 = \sigma^2$, and define G as the normal distribution, adopting the notation $X(0) \sim \mathcal{N}(\mu, \sigma^2)$.

(ii) Given the characteristic polynomial P of $X(0)$ and its derivative Q, $X(0)$ has distinct eigenvalues (and hence $\lambda_1 \neq \lambda_2$) provided the P and Q do not share a common root. P and Q have a common root when the determinant

of the Sylvester matrix composed of P and Q is zero. The determinant is a multivariate polynomial in entries of P and Q and is non-trivial, as there exist symmetric matrices with distinct eigenvalues, hence the set of matrices for which this determinant is zero has Lebesgue measure zero. Assuming $X(0)$ is drawn from a distribution that assigns probability zero to matrix sets of Lebesgue measure zero, it follows in probability that P and Q do not share a common root, and that every eigenvalue of $X(0)$ is distinct. Hence $\lambda_1 \neq \lambda_2$ and, where λ_1 denotes the largest eigenvalue, $\lambda_1 > \lambda_2$.

(iii) If $\mathbf{q}_1$ contains a zero at index i, then defining $\tilde{\mathbf{q}}_1 \in \mathbb{R}^{n-1}$ as $\mathbf{q}_1$ with the i-th entry removed, and $\tilde{X}(0) \in \mathbb{R}^{(n-1)\times(n-1)}$ as $X(0)$ with the i-th row and column removed, $\tilde{\mathbf{q}}_1$ is an eigenvector of $\tilde{X}(0)$ corresponding to the same eigenvalue. Hence the corresponding characteristic polynomials P and $\tilde{P}$ share a common root, in which case the determinant of the Sylvester matrix composed of P and $\tilde{P}$ is zero. By the same argument used for condition (ii), the set of matrices that satisfy this requirement has Lebesgue measure zero. Hence it follows in probability that all entries of $\mathbf{q}_1$ are non-zero.

It is noted that both (ii) and (iii) hold for all n, whereas (i) holds in the large-n limit. Provided condition (iii) holds, the positive and negative index sets of the eigenvector $\mathbf{q}_1$, given by $S = \{k : q_{1k} > 0\}$ and $T = \{k : q_{1k} < 0\}$ respectively, partition the vertex indices into two opposing cliques of friends which, via the Structure Theorem, instantiate a balanced graph. Thus the paper [19] concludes that provided conditions (i)-(iii) hold, which they do with probability one in the large-n limit, the system (3.2) will bring an initial random matrix to a balanced state in finite time.

3.1.2 Forward Euler scheme

We use a forward Euler scheme to verify the results in [17] and [19]. Noting the convergence results and conditions from the previous sections, for large n we define convergence as *a balanced complete graph as time approaches* $t^* = 1/\lambda_1$. This is given (with high probability in large n) that the largest eigenvalue λ_1 of $X(0)$ is simple and positive, and the associated eigenvector contains no zero entries. The

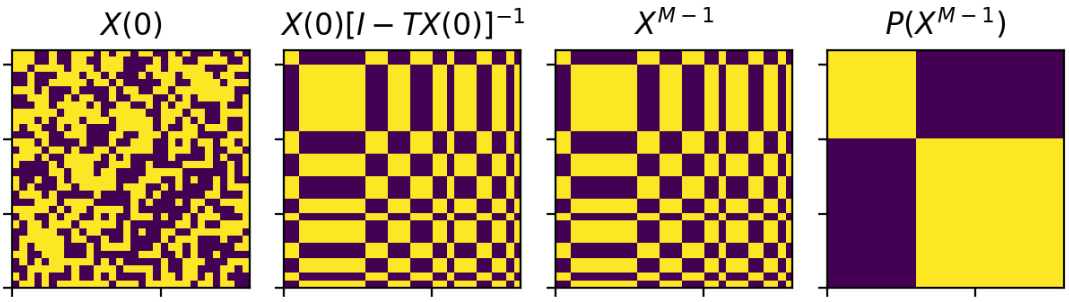

Figure 3.1: Agreement between analytic and numerical solutions to (3.2) (centre), given symmetric initial conditions drawn from a standard normal distribution $X(0) \sim \mathcal{N}(0, 1)$ (left). Yellow indicates positive entries and purple negative entries. A permutation of the index set of vertices, $P(\cdot)$, illustrates that the end-state has a balanced sign structure by Theorem 3. Plotted in Python with $n = 16$.

numerical solutions are obtained with the time discretisation $\Delta t = t^*/M$ such that $X^m = X(m\Delta t)$ with

$$t_m = m\Delta t, \quad m = 0, 1, \ldots, M-1, \tag{3.16}$$

and instantiating a forward Euler scheme,

$$X^{m+1} = X^m + F(X^m)\Delta t. \tag{3.17}$$

Figure 3.1 compares the analytic solution (3.12) and numerical solution (3.17), illustrating the sign structure of X at a time just before the singularity at $t = t^*$. These 'final states' are plotted at $T = t^* - \epsilon$ and $t = (M-1)\Delta t$ for the analytic and numerical solutions respectively. A permutation of the final state shows that the sign structure satisfies the Structure Theorem, hence the graph is balanced. Note here that $n = 16$, resulting in factions of different sizes. For larger n the factions in the end state tend to equal size, see [19] for proof.

The associated dynamics of $X(t)$ under the Kułakoski model (3.2) are shown for $t \in [0, t^*)$ in Figure 3.2. The results are illustrated for initial distributions with means 0 and 1, which result in bipolar and consensus final states respectively, consistent with [19].

It is proven in [19] that $X(t)$ converges to a rank-one matrix for symmetric initial conditions, corresponding to an undirected graph. Traag *et al.* [20] show

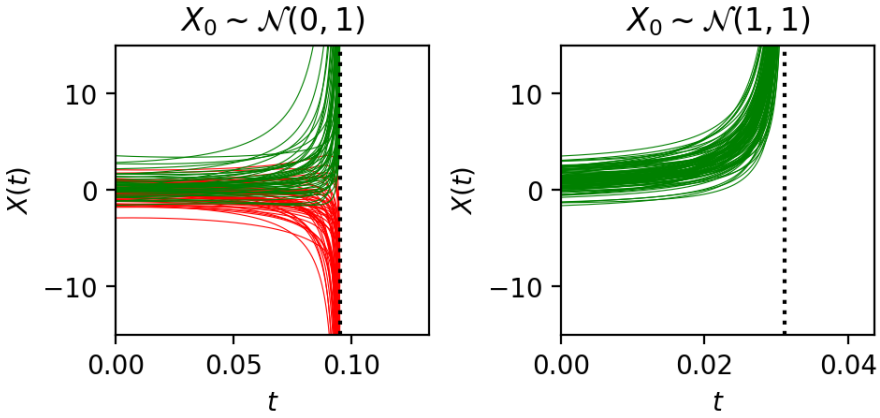

Figure 3.2: Numerical dynamics of the entries of $X(t)$ under (3.2), coloured green (positive) and red (negative) corresponding to the sign of the entry on approaching $t^* = 1/\lambda_1$, shown as a dotted black line. The resulting balanced states are bipolar for $\mu = 0$ (left) and consensus for $\mu = 1$ (right). Plotted in Python with $n = 32$.

that this is also the case for normal initial conditions. They later show that convergence does not happen, in general, for non-normal initial conditions (and hence directed graphs in general), a proof of which is outlined in [20].

3.2 Model for directed graphs

Traag *et al.* [20] propose an alternative initial value problem that converges to balance for directed graphs, given by

$$\dot{X} = XX^T, \quad X(0) = X_0, \tag{3.18}$$

or, in elementwise notation,

$$\dot{X}_{ij} = \sum_{k \in V} X_{ik} X_{jk}, \quad i, j \in V. \tag{3.19}$$

In the context of the earlier interpretation of the dynamics representing gossiping mechanisms, here vertex i considers j's opinion of all the vertices k in the graph and updates its opinion of j accordingly.

Although the interpretation of this alternative mechanism is not as intuitive from a gossiping perspective, it is proven in [20] that $X(t)$ converges to a symmetric

rank-one matrix for the initial value problem (3.18) with generic, non-normal initial conditions, $X_0 \in \mathbb{R}^{n\times n}$. The proof relies on the fact that the differential equation is symmetric and that any matrix may be decomposed into symmetric and skew-symmetric components, $X(t) = S(t) + A(t)$. As XX^T is symmetric the flow only acts on the symmetric components of X, where skew-symmetric components remain constant, given by A_0. The solution hence takes the form

$$X(t) = S(t) + A_0, \tag{3.20}$$

where $S(t)$ can be found by letting $\hat{S} = e^{-tA_0} S e^{tA_0}$ and solving

$$\dot{\hat{S}} = \hat{S}^2 - A_0, \quad \hat{S}(0) = S_0. \tag{3.21}$$

Under specific conditions outlined in [20], the growth of the symmetric component then drives the entire solution to a state of balance.

3.2.1 Numerical comparisons

Here we replicate and compare numerical solutions to the models presented in [17] and [20], $F(X) = X^2$ and $F(X) = XX^T$ respectively. For symmetric initial conditions, symmetry is preserved under both flows, hence $X(t) = X(t)^T \ \forall\, t$, in which case the solutions under both models are identical, driving the graph to the same balanced state as shown in Figure 3.3. This is of course not the case for non-symmetric initial conditions where, as mentioned in the previous section, only the latter reaches a balanced state, shown in Figure 3.4.

We note a lack of qualitative explanations in the literature as to why only the latter model drives non-symmetric initial conditions to balance. We suggest one here. In the former model $F(X) = X^2$, the product $X_{ik}X_{kj}$ which guides X_{ij} towards balancing the triad $\triangle_{ijk}$ accounts for paths in one direction only: from i to k to j. The latter model is bidirectional, owing to the presence of X^T, driving balance in both directions and hence leading asymmetric graphs to states of balance. We found and verified computationally that other permutations of the above models lead to balance for asymmetric initial conditions, provided they contain a factor of X^T, e.g. $(X^T)^2$, $X^T X$.

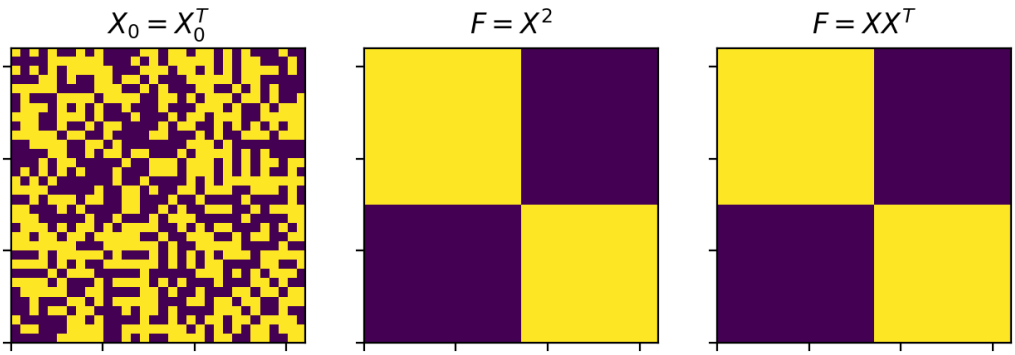

Figure 3.3: Comparison of the convergence for symmetric initial conditions. The index set of vertices is permuted in the final states to yield the illustrated block sign structure, showing both models are balanced. Plotted in Python for $n = 32$.

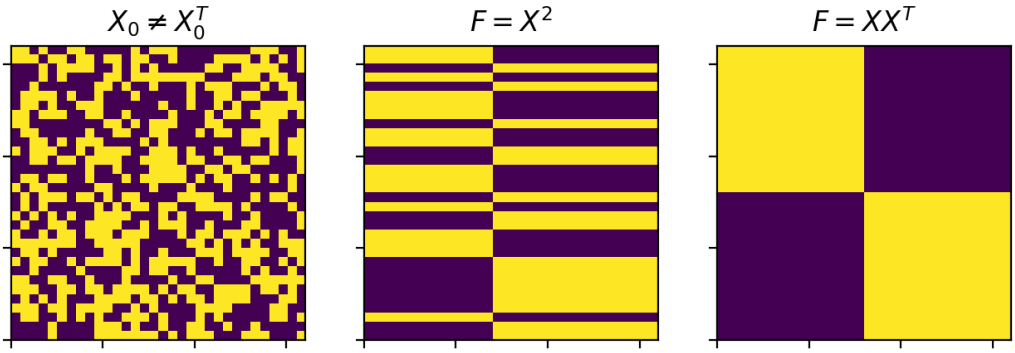

Figure 3.4: Comparison of the convergence for generic non-symmetric initial conditions. Here, only the model $F(X) = XX^T$ converges to balance. Plotted in Python for $n = 32$.

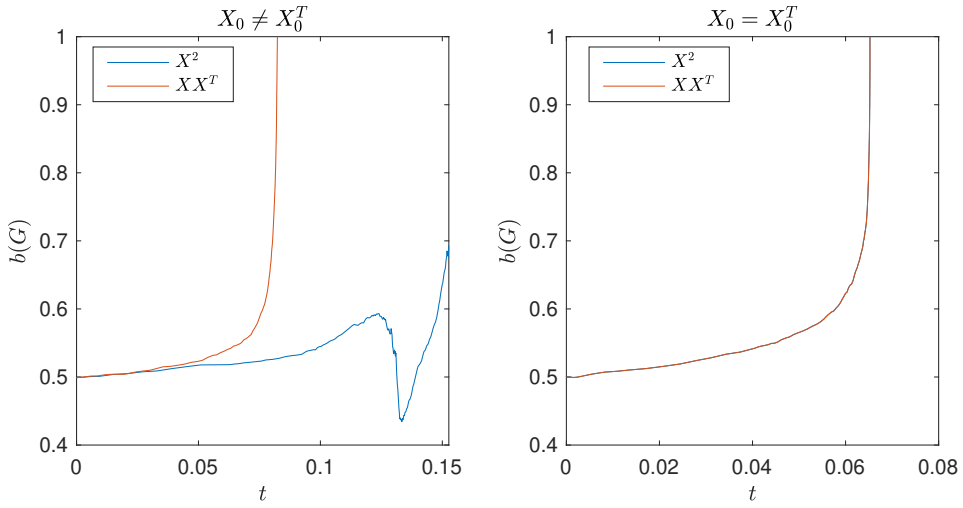

Figure 3.5: Time dynamics of balance of for $F(X) = X^2$ [17] and $F(X) = XX^T$ [20] models, for non-symmetric initial conditions (left) and symmetric initial conditions (right). In the non-symmetric instance, the former model fails to converge to balance with a final state of $b(G) \approx 0.7$ at the singularity.

The dynamics of the degree of balance $b(G)$ under each model is shown in Figure 3.5 for symmetric and non-symmetric initial conditions, from which we can also infer the rate at which the model drives the graph towards balance. As noted, the dynamics are identical for symmetric initial conditions and only the model $F(X) = XX^T$ drives the graph to balance for non-symmetric initial conditions, indicated by $b(G) = 1$. In cases where balance is achieved, the rate of change of balance increases as the graph becomes more balanced, reflecting increased coherence of influence and pressures to conform within the graph, as we argued is a benefit of continuous models in earlier sections.

3.2.2 Behaviour on other graph topologies

A natural progression of the above work is to consider dynamics on other graph topologies. However, the convergence conditions outlined earlier and in [19] for a balanced, fully connected end-state still hold. Thus, provided that the graph is not disconnected and satisfies such conditions, the graph will still converge. This is demonstrated on a signed triangular lattice with periodic boundary conditions. In two dimensions, this defines a triangulation of a torus, which we define as the

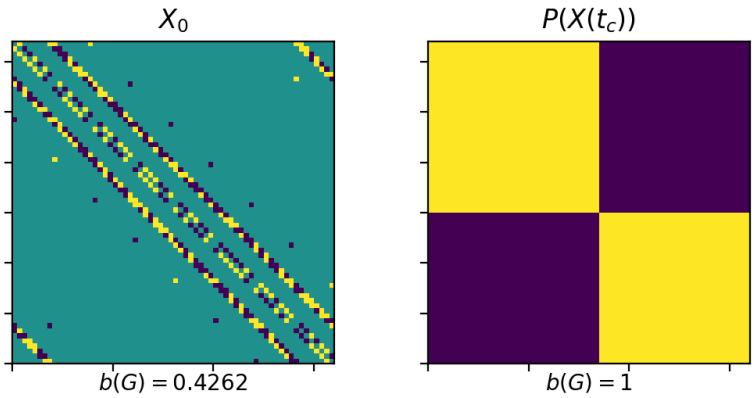

Figure 3.6: Form of X_0 representing a non-symmetric torus triangulation (left), corresponding to a triangular lattice with periodic boundary conditions, and the resultant balanced state at the singularity under the flow $F(X) = XX^T$ (right). Shown below each plot is the degree of balance $b(G)$. Green indicates no edge, i.e. a weight of 0. $n = 64$.

non-symmetric edge-set $\mathcal{T}$, and draw the edge weights from a normal Gaussian distribution,

$$\begin{aligned} X_{ij} &\sim \mathcal{N}(0,1), \quad && (i,j) \in \mathcal{T} \\ X_{ij} &= 0, && (i,j) \notin \mathcal{T}. \end{aligned} \tag{3.22}$$

As the graph is not disconnected and the distribution of the entries of $X(t)$ is symmetric about zero, by the conclusions from [19] and [20] we expect the flow $\dot{X} = XX^T$ to drive the initial condition to a fully connected, balanced, bipolar state. The (non-symmetric) triangular lattice adjacency matrix is generated in code for any n, and the resultant balanced state is computationally verified, as shown for $n = 64$ in Figure 3.6.

3.2.3 The symmetry of end states

We note that even for non-normal initial conditions, the final (balanced) state under the model (3.18) is symmetric [20]. This is consistent with the graph-theoretic formulation of structural balance as first investigated by Harary-Cartwright [15]. They conclude therein that whenever the edges X_{ij} and X_{ji} are of different signs, the signed graph containing them is not balanced. Hence, even for asymmetric initial conditions, it is a necessary condition that the final state is symmetric.

Although the model $\dot{X} = XX^T$ is interesting from a directed graph perspective, we limit many of our further investigations to the symmetric case with the associated model $\dot{X} = X^2$. The motivation for this is two-fold. The first is that symmetry of relations is a necessary condition for a balanced graph, as outlined above. The second is sociological, in that humans are typically effective at perceiving positive and negative sentiments of others, such that relations between individuals have a natural tendency toward symmetry [31].

3.3 Other models

Another model is that of Shang *et al.* [32], who argue that vertices do not perceive the opinions of others perfectly, due to normative pressure in the social environment or the persistence of initial impressions. Hence a discrepancy between real sentiment X and "perceived sentiment" $\hat{X}$ is encountered, and the latter is modelled as a combination of actual sentiment and an 'outside influence' matrix.

Wongkaew *et al.* [29] investigate an optimal control strategy of the modified system (3.4) through the use of a leader vertex which steers the dynamics towards a state of consensus. The leader is denoted as the zeroth vertex in the following control system with initial conditions $X(0) = X_0$ and $u(0) = u_0$,

$$\begin{aligned} \dot{X}_{0i} &= u_i(t), \\ \dot{X}_{ij} &= \frac{1}{n-2}\left(1 - \frac{X_{ij}^2}{R^2}\right) \sum_{k \in V \setminus \{i,j\}} X_{ik}X_{kj} + \gamma X_{0i}X_{0j}, \end{aligned} \tag{3.23}$$

where γ is a static control parameter and the control variable $u_i(t)$ represents the prescribed edge weight between the leader and vertex i.

The optimal control $u_i(t)$ driving the graph to a state of balance is then determined by defining a cost functional J which is minimised subject to the initial value problem (3.23) using a Runge-Kutta scheme and conjugate gradient method.

A drawback of this method however is that it can drive the graph to consensus, but not to bipolarity. This limitation is overcome by a control model we introduce in later sections.

In this chapter we investigated existing unbounded models in continuous time, numerically replicating the dynamics which diverge at a time $t^* = 1/\lambda_1$ and outlining the associated conditions required for the graph to tend to a state of balance. The behaviour over different linear graph topologies is the same, provided the graph is not disconnected, and we illustrate an example of this. We provide a qualitative argument for why a model on directed graphs leads to a state of balance. However, we note that at a balanced state relations must be symmetric, and hence we motivate our focus on the model $\dot{X} = X^2$. This model forms a base from which we consider various extensions, outlined in the following chapter.

Chapter 4

Model extensions

In this chapter we present extensions of the Kułakowski model [17] on undirected graphs, i.e. $X_0 = X_0^T$. We first include a factor of $1/n$ in the basic model, accounting for the size of the graph which we use going forward,

$$\dot{X} = F(X) = \frac{1}{n}X^2, \quad X(0) = X_0, \tag{4.1}$$

or, in elementwise form,

$$\dot{X}_{ij} = F_{ij}(X) = \frac{1}{n}\sum_{k\in V} X_{ik}X_{kj}, \quad i,j \in V. \tag{4.2}$$

This slows the dynamics, the solution following eigendecomposition being dominated by the leading eigenvalue,

$$\Lambda_{11}(t) = \frac{\lambda_1}{1 - \frac{\lambda_1}{n}t}, \tag{4.3}$$

with the singularity now located at $t^* = n/\lambda_1$.

To prove that t^* is finite for large n we need to know the dependence of λ_1 on n. In the case where X_0 is a symmetric Gaussian matrix with iid entries of mean zero and variance one (for $i \leq j$), we use the result from Bai and Yin [33] that the eigenvalue distribution of $X_0/\sqrt{n}$ converges to Wigner's semi-circle distribution on $[-2, 2]$ with probability one, hence

$$\lim_{n\to\infty} \frac{\lambda_1}{\sqrt{n}} = 2. \tag{4.4}$$

As the largest eigenvalue scales as $\lambda_1 \sim 2\sqrt{n}$ in probability, then $t^* \sim \sqrt{n}/2$. We conclude that provided n is large but finite, the conditions required for convergence outlined in Section 3.1.1 still hold for (4.1). This argument also connects the numerical results of [17], $t^* \propto n^{-1/2}$, with the arguments in [19], $t^* = 1/\lambda_1$.

4.1 Dynamics with saturation

With an appropriate non-linear modification of the system, the dynamics may be bounded (smoothly) to some prescribed range $[-R, R]$, as in [17, 29]. This is done previously without considering self-loops, i.e. $X_{ii} = 0, \forall i \in V$. To bound the dynamics of (4.3), we outline the analogous model which includes self-loops. In elementwise notation, this is given by,

$$\dot{X}_{ij} = M_{ij}(X) = \left(1 - \frac{X_{ij}^2}{R^2}\right) F_{ij}(X), \quad i, j \in V. \tag{4.5}$$

where F_{ij} is ij-th entry of one of the dynamics discussed previously. By including self-loops we can also define the model in matrix notation,

$$\dot{X} = \left(\mathbf{1}_{n\times n} - \frac{X \odot X}{R^2}\right) \odot F(X), \tag{4.6}$$

where $\mathbf{1}_{n\times n}$ denotes a matrix of ones and $\odot$ the elementwise product. The forward Euler solution for various initial conditions is shown in Figure 4.1. As the singularity in the original system has been removed by the nonlinear modification, we now refer to t^* as the time the graph 'saturates' at a balanced steady-state.

4.1.1 Convergence

The condition for convergence to a balanced state for the model (4.5) excluding self-loops is outlined in a paper by Wongkaew *et al.* [29], and given by

$$X_{ij}(0) > -R, \quad \forall\, i, j \in V, \tag{4.7}$$

however, we found this to be incorrect: we provide here a case which satisfies (4.7) but does not result in a balanced graph. We then reformulate the arguments in [29] into two lemmas that acknowledge this correction. This is applied to graphs containing self-loops, not requiring zero entries on the diagonal.

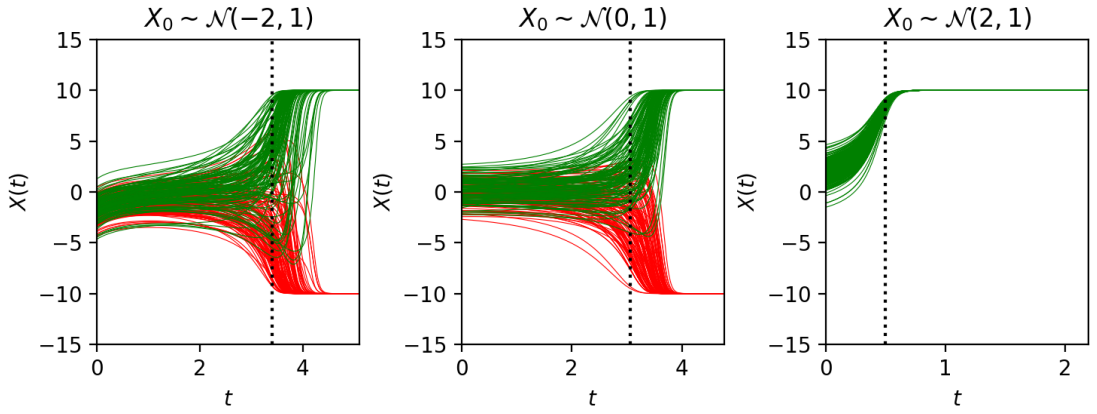

Figure 4.1: Forward Euler solution to (4.6) for a range of symmetric initial conditions with $R = 10$, $n = 32$. The singularity of the unbounded model $t = n/\lambda_1$ is shown as a dotted black line, illustrating that the non-linear modification slows down the dynamics.

Consider an initial constant matrix, $X_{ij} = a \; \forall \, i, j \in V$, where $-R < a < 0$. In this case every entry of X uniformly tends to zero from below, corresponding to a fully disconnected graph. This is proven as follows. First we note that the set of constant matrices $\mathcal{C} = \{a\mathbf{1}_{n\times n} \,|\, a \in \mathbb{R}\}$ is invariant under the flow (4.6),

$$\begin{aligned} M(a\mathbf{1}_{n\times n}) &= \left(\mathbf{1}_{n\times n} - \frac{a^2}{R^2}\mathbf{1}_{n\times n}\right) \odot \frac{1}{n}a^2\mathbf{1}^2_{n\times n} \\ &= \left(1 - \frac{a^2}{R^2}\right)\frac{1}{n}a^2\mathbf{1}^2_{n\times n} \\ &= \left(1 - \frac{a^2}{R^2}\right)a^2\mathbf{1}_{n\times n} \;\in \mathcal{C}, \end{aligned} \tag{4.8}$$

noting $\mathbf{1}_{n\times n} \odot \mathbf{1}_{n\times n} = \mathbf{1}_{n\times n}$ and $\mathbf{1}^2_{n\times n} = n\mathbf{1}_{n\times n}$. Hence it suffices to solve the scalar initial value problem,

$$\dot{x} = \left(1 - \frac{x^2}{R^2}\right)x^2, \quad x(0) = a. \tag{4.9}$$

which has fixed points at $x^* = \{-R, 0, R\}$. To study how x approaches zero from below, let $x \sim \epsilon$ where $|\epsilon| \ll 1$, such that

$$\dot{x} \sim x^2 + \mathcal{O}(x^4) \tag{4.10}$$

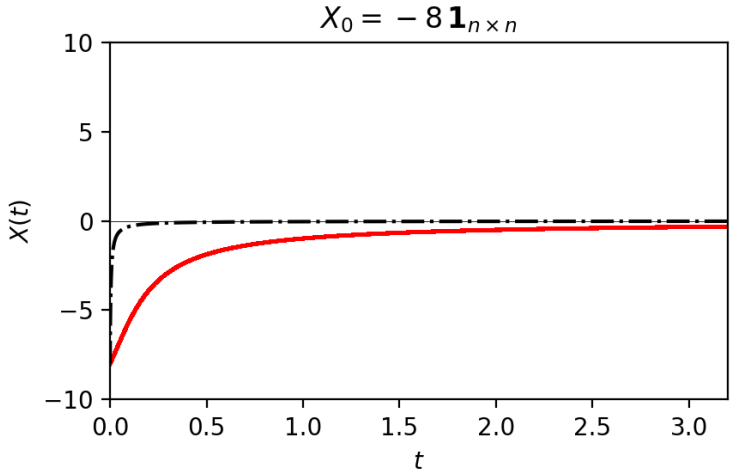

Figure 4.2: Plot of the case contradicting the condition (4.7). Here $R = 10$, hence $X_0 = -8\,\mathbf{1}_{n\times n} > -R\,\mathbf{1}_{n\times n}$, satisfying (4.7). However, the numerical solution of the full system (red) approaches zero from below, converging to the asymptotic solution (4.11) (black-dashed), instead of a balanced state with entries $X_{ij} = \pm R$.

Hence as $x \to 0$, the solution asymptotically approaches,

$$x(t) \sim \frac{a}{1 - at}, \tag{4.11}$$

which, for $a < 0$, it is clear that this converges to zero at leading order. Hence every entry of the matrix $X = a\mathbf{1}_{n\times n}$ converges uniformly to zero for $-R < a < 0$. In the case of $a > 0$, the matrix converges to a balanced state of consensus, $X = R\,\mathbf{1}_{n\times n}$. We illustrate the former case computationally in Figure 4.2, showing that it converges to the asymptotic solution (4.11).

With this result in mind, we reformulate the propositions in [29] correctly and apply them to graphs with self-loops in the following two lemmas.

Lemma 4. *Given a connected graph $X_{ij}(0) \in (-R, R)$, $\forall\, i, j \in V$ and $X(0) = X(0)^T$, then for $t < t^*$ the following result holds under the flow (4.6) with $F(X) = \frac{1}{n}X^2$,*

$$\frac{\mathrm{d}}{\mathrm{d}t} X_{ij}(t)X_{ik}(t)X_{kj}(t) > 0, \quad \forall\, i, j, k \in V, \tag{4.12}$$

where i, j, k are not necessarily distinct.

Proof.

$$\begin{aligned}\frac{\mathrm{d}}{\mathrm{d}t}\sum_{i,j,k\in V} X_{ij}X_{ik}X_{kj} &= \sum_{i,j,k\in V}\left(\dot{X}_{ij}X_{ik}X_{kj} + X_{ij}\dot{X}_{ik}X_{kj} + X_{ij}X_{ik}\dot{X}_{kj}\right)\\ &= \frac{1}{n}\sum_{i,j\in V}\left(1-\frac{X_{ij}^2}{R^2}\right)\left(\sum_{k\in V} X_{ik}X_{kj}\right)^2\\ &\quad + \frac{1}{n}\sum_{i,k\in V}\left(1-\frac{X_{ik}^2}{R^2}\right)\left(\sum_{j\in V} X_{ij}X_{jk}\right)\left(\sum_{j\in V} X_{ij}X_{kj}\right)\\ &\quad + \frac{1}{n}\sum_{k,j\in V}\left(1-\frac{X_{kj}^2}{R^2}\right)\left(\sum_{i\in V} X_{ki}X_{ij}\right)\left(\sum_{i\in V} X_{ij}X_{ik}\right). \quad (4.13)\end{aligned}$$

As the set of symmetric matrices X is invariant under $F = X^2$, given symmetric initial conditions, $X_{ij}(t) = X_{ji}(t)$, $\forall\, t \in [0,\infty)$, hence

$$\begin{aligned}\frac{\mathrm{d}}{\mathrm{d}t}\sum_{i,j,k\in V} X_{ij}X_{ik}X_{kj} &= \frac{1}{n}\sum_{i,j\in V}\left(1-\frac{X_{ij}^2}{R^2}\right)\left(\sum_{k\in V} X_{ik}X_{kj}\right)^2\\ &\quad + \frac{1}{n}\sum_{i,k\in V}\left(1-\frac{X_{ik}^2}{R^2}\right)\left(\sum_{j\in V} X_{ij}X_{kj}\right)^2\\ &\quad + \frac{1}{n}\sum_{k,j\in V}\left(1-\frac{X_{kj}^2}{R^2}\right)\left(\sum_{i\in V} X_{ij}X_{ik}\right)^2. \quad (4.14)\end{aligned}$$

Provided $|X_{ij}| < R$, $\forall\, i,j \in V$ and the graph is connected, the above term is strictly increasing. This occurs until the graph reaches a fixed point $|X_{ij}| = R$ or $|X_{ij}| = 0\ \forall\, i,j \in V$ at a time denoted t^*. □

Note that the statement (4.12) does not imply the graph ultimately reaches a state of balance. As proven, the trivial fixed point $X^* = \mathbf{0}_{n\times n}$, corresponding to a graph with no edges, is an ω-limit point for all $X_{ij} = a\ \forall\, i,j \in V$, where $-R < a < 0$, but it converges such that (4.12) holds for $t \in [0,\infty)$. The following lemma, also a corrected reformulation of a proposition in [29], shows that if at some point the graph in fact reaches balance, then either $-R$ or R is an ω-limit point for each entry X_{ij}. We also prove this for graphs containing self-loops.

Lemma 5. *If a fully connected graph G is balanced, then under the dynamics (4.6), for each entry of X, one of the points $\{-R, R\}$ is an ω-limit point, i.e. the following limit holds,*

$$\lim_{t\to\infty} X_{ij}(t) = \pm R, \quad \forall\, i, j \in V. \tag{4.15}$$

Proof. Define the potential

$$V(x) = \frac{1}{4}\sum_{i,j\in V}(X_{ij}^2 - R^2)^2 \tag{4.16}$$

and take the derivative with respect to time,

$$\begin{aligned}\dot{V} &= \sum_{i,j\in V}(X_{ij}^2 - R^2)X_{ij}\dot{X}_{ij} \\ &= \frac{1}{n}\sum_{i,j\in V}(X_{ij}^2 - R^2)X_{ij}\left(1 - \frac{X_{ij}^2}{R^2}\right)\sum_{k\in V}X_{ik}X_{kj} \\ &= -\frac{1}{nR^2}\sum_{i,j\in V}(X_{ij}^2 - R^2)^2\sum_{k\in V}X_{ij}X_{ik}X_{kj}.\end{aligned} \tag{4.17}$$

If G balanced and fully connected, $X_{ij}X_{ik}X_{kj} > 0$, $\forall\, i, j, k \in V$, and hence $\dot{V} \leq 0$. If $|X_{ij}| \neq R$ for any $i, j \in V$, then $\dot{V} < 0$. Hence the limit (4.15) holds. □

The additional factor of $1/2$ in $V(x)$ accounts for the fact that the graph is undirected, such that each edge represented in the symmetric matrix X is only counted once. The reason Lemma 5 is not applicable in the previously discussed case of $X = a\mathbf{1}_{n\times n}$ for $-R < a < 0$ is that no graph containing equally weighted negative edges is considered balanced, nor will such a graph reach a state of balance as it asymptotically approaches $\mathbf{0}_{n\times n}$ from below. Thus the result of Lemmas 4 and 5 is that under the model (4.6), provided $|X_{ij}| < R\ \forall\ i, j \in V$, a connected graph tends towards a state of balance and, provided the graph in fact reaches a balanced state, the edges converge to a value of $\pm R$, corresponding to a balanced fixed point.

4.1.2 Stability of utopian and dystopian states

Wongkaew *et al.* [29] also perform a local analysis around two specific fixed points: all positive and all negative relations, i.e. $X_{ij}^* = R$ and $X_{ij}^* = -R$, for all

$i, j \in V \setminus \{i = j\}$, corresponding to balanced 'utopia' and imbalanced 'dystopia' respectively. To do so, the authors vectorise the matrix system and analyse the associated Jacobian. We outline a similar proof including self-loops in the following section, as it provides a basis for us to then prove the stability of all balanced fixed points in general. However, we first note that there is a more straightforward way of assessing the stability of the specific two fixed points addressed in [29] when we include self-loops: it allows us to investigate the case $X^* = \pm R\,\mathbf{1}_{n\times n} \in \mathcal{C}$, for which we can simply analyse the Jacobian of the reduced system (4.9) at $x^* = \pm R$,

$$J(x) = 2x - \frac{4}{R^2}x^3, \tag{4.18}$$

for which $J(\pm R) = \mp 2R$. Hence $X^* = R\,\mathbf{1}_{n\times n}$ is stable and $X^* = -R\,\mathbf{1}_{n\times n}$ is unstable. This is verified computationally and illustrated in Figure 4.3. This is a reasonable result, as we know from Lemma 4 that the system drives the graph towards a balanced state; the utopian fixed point $X^* = R\,\mathbf{1}_{n\times n}$ is already in a state of balance, whereas the dystopian fixed point is imbalanced.

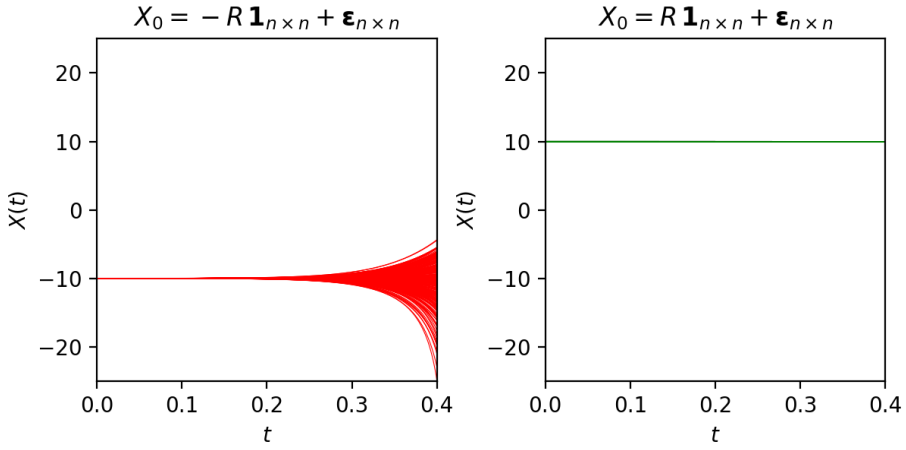

Figure 4.3: Stability of fixed points $X^* = \pm R\,\mathbf{1}_{n\times n}$ with $R = 10$ and $n = 32$. The system (4.6) is initialised at the fixed point with a small perturbation matrix with entries $\varepsilon_{ij} \overset{iid}{\sim} \mathcal{N}(0, 0.001)$. The numerics indicate that $X^* = -R\,\mathbf{1}_{n\times n}$ is unstable and $X^* = R\,\mathbf{1}_{n\times n}$ is stable, in agreement with analytic results.

4.1.3 Stability of all balanced fixed points

We first show an alternative proof of stability around the two fixed points $X^* = \pm R\,\mathbf{1}_{n\times n}$. This provides a natural basis for consideration of the stability of balanced fixed points in general. Recalling the elementwise form of the system is

$$M(X_{ij}) = \frac{1}{n}\left(1 - \frac{X_{ij}^2}{R^2}\right)\sum_{k\in V} X_{ik}X_{kj}, \tag{4.19}$$

we can vectorise the system, similar to [29] but including diagonal entries corresponding to self-loops. In our symmetric setting we vectorise the upper triangular component of X row-wise. The resulting vector of length $K = n(n+1)/2$ has the structure,

$$\mathcal{X} = (X_{11}, \ldots, X_{1n}, X_{22}, \ldots, X_{2n}, \ldots, X_{(n-1)(n-1)}, X_{(n-1)n}, X_{nn}) \in \mathbb{R}^K. \tag{4.20}$$

Let T be the index set of pairs where $(i,j) \in T$ covers the upper triangular component of X such that $|T| = K$, the pairs ordered as in $\mathcal{X}$ above. Letting $M(X_{ij}) = M_{ij}$, in defining entries of the Jacobian $J \in \mathbb{R}^{K\times K}$ below we maintain the matrix indexing, differentiating with respect to X_{pq}, where $(p,q) \in T$. Diagonal terms of the Jacobian hence correspond to $(i,j) = (p,q)$.

$$\frac{\partial M_{ij}}{\partial X_{pq}} = \frac{1}{n}\frac{\partial}{\partial X_{pq}}\left(1 - \frac{X_{ij}^2}{R^2}\right)\sum_{k\in V} X_{ik}X_{kj} + \frac{1}{n}\left(1 - \frac{X_{ij}^2}{R^2}\right)\frac{\partial}{\partial X_{pq}}\sum_{k\in V} X_{ik}X_{kj} \tag{4.21}$$

At the two fixed points, $X^* = \pm R\,\mathbf{1}_{n\times n}$, the second term in the above equation is zero and the summation contained in the first term is nR^2. The first term is only non-zero when $(i,j) = (p,q)$,

$$\frac{\partial M_{ij}}{\partial X_{pq}}\Big|_{X_{ij}=\pm R} = \begin{cases} \mp 2R, & (i,j) = (p,q) \\ 0, & \text{otherwise} \end{cases}. \tag{4.22}$$

Thus nonzero cases correspond to diagonal entries, hence the Jacobian is

$$J(\pm R\,\mathbf{1}_{n\times n}) = \mp 2R\, I_K, \tag{4.23}$$

where I_K is the identity matrix. As the diagonal entries are equal to the eigenvalues, $X^* = R\,\mathbf{1}_{n\times n}$ is stable and $X^* = -R\,\mathbf{1}_{n\times n}$ is unstable, consistent with our earlier conclusions.

We now classify the stability of the fixed points $X^* \in \mathcal{B}$ which correspond to the balanced states of the system, showing that all of them are stable. The challenge here is in inferring the sign of the summation

$$\sum_{k \in V} X_{ik} X_{jk}, \tag{4.24}$$

which dictates the sign of the corresponding entry in the Jacobian. First note that X is symmetric, hence the above summation is equivalent to an inner product of the rows i and j. We observe that in a balanced state, if vertices i and j belong to the same faction, then their opinions of others (and themselves) are coherent. The opposite is true if they belong to separate factions. Hence given the vertices are members of the factions $i \in V_1$ and $j \in V_2$, we conclude that if a fixed point is balanced, then

$$\sum_{k \in V} X_{ik} X_{jk} = \begin{cases} nR^2, & V_1 = V_2 \\ -nR^2, & V_1 \neq V_2 \end{cases}. \tag{4.25}$$

This is consistent with the Structure Theorem 3. Now note that at a fixed point, $X_{ij} = R$ if i and j belong to the same faction, i.e. $V_1 = V_2$, and $X_{ij} = -R$ otherwise. Hence the product of X_{ij} and the above sum is positive for all $X^* \in \mathcal{B}$. Therefore the entries of the Jacobian (4.21) are given by

$$\frac{\partial M_{ij}}{\partial X_{pq}}\Big|_{X_{ij}=\pm R} = \begin{cases} -2R, & (i,j) = (p,q) \\ 0, & \text{otherwise} \end{cases}, \quad \forall\, X^* \in \mathcal{B}. \tag{4.26}$$

Hence X^* is stable for all $X^* \in \mathcal{B}$. This is verified numerically, shown in Figure 4.4. This is a reasonable result when considered from the context of Lemmas 4 and 5, where we know if a graph is balanced and the entries are in the appropriate range, then X will tend towards a fixed point $X^* \in \mathcal{B}$. Hence the conclusion that such fixed points are stable is justified.

In this section, we investigated an existing model with bounded dynamics (4.6). We outlined Lemmas 4 and 5 as corrections to propositions made by Wongkaew *et al.* [29], outlining the conditions for the bounded dynamics to reach a balanced fixed point. The authors in [29] also prove the stability of two fixed points corresponding to all-positive or all-negative graphs, but we do better. Here we generalise our earlier proofs for the stability of $X^* = \pm R\, \mathbf{1}_{n \times n}$ to characterise the

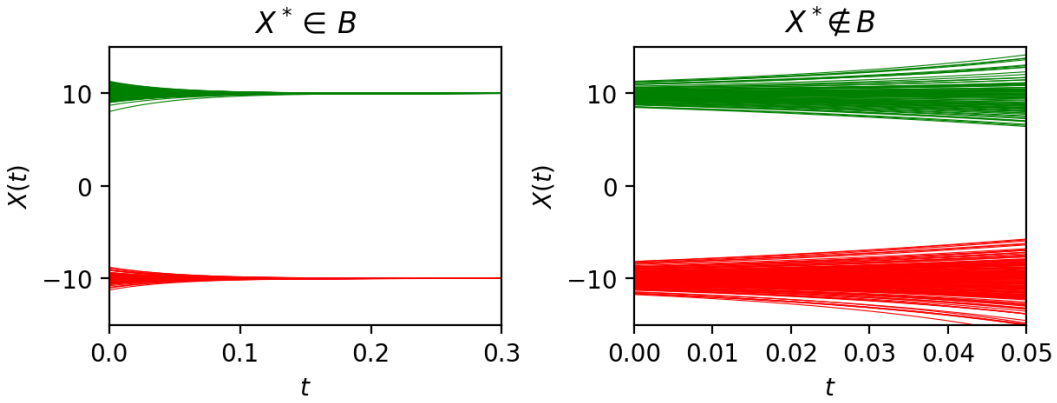

Figure 4.4: Stability of a balanced-state fixed point, $X^* \in \mathcal{B}$, each entry perturbed by $\epsilon_{ij} \overset{iid}{\sim} \mathcal{N}(0, 0.5)$. The instability of an imbalanced fixed point is also shown.

stability of all balanced fixed points, showing that they are all stable. We connect this finding to Lemmas 4 and 5. The generalisation to balanced fixed points is achieved by our observation that the inner product of rows i and j is negative if the corresponding vertices belong to different factions, and positive if they belong to the same faction.

We now utilise these findings for further extensions based on static control and a multiplex topology. To our knowledge, we present such models in the following sections as novel contributions.

4.2 Static control model

In this section, we present a control model (4.27) which can steer the graph towards a desired balanced state. The control is determined by a desired balanced fixed point, denoted as $X^* = \mathbf{v}\mathbf{v}^T$, and parameterised with $\beta \in [0, 1]$. Ideally $\beta \ll 1$, the control serving to nudge the system via a small perturbation onto a trajectory that leads the system to the desired state. The model is given by

$$\dot{X} = C(X; R) \odot \left[(1 - \beta)F(X) + \beta(\mathbf{v}\mathbf{v}^T - X)\right]. \tag{4.27}$$

This has the advantage that the desired end-state (bipolar or utopia) and, more specifically, the clique to which each vertex belongs, may be prescribed by the modeller by prescribing $\mathbf{v}$.

The prescription of the balanced end-state of the graph is achieved by assigning positive or negative entries to the state vector $\mathbf{v} \in \mathbb{R}^n$. In the case of a (maximal) 2 cliques in the end state, vertices belonging to the same clique will carry the same sign in the corresponding entry of $\mathbf{v}$, as illustrated below. The factor $\sqrt{R}$ ensures that $X^* = \mathbf{v}\mathbf{v}^T$ is a fixed point of the system (4.27).

$$\begin{pmatrix} \text{Faction A} \\ \text{Faction B} \\ \vdots \\ \text{Faction A} \end{pmatrix} \implies \mathbf{v} = \sqrt{R} \begin{pmatrix} +1 \\ -1 \\ \vdots \\ +1 \end{pmatrix} \tag{4.28}$$

Figures 4.5-4.8 illustrate that the graph may be steered to bipolar or consensus states, defined by the target steady-state $X^* = \mathbf{v}\mathbf{v}^T$. We define the cut-off time $t_c > t^*$, chosen arbitrarily once the dynamics reach a steady state.

The key benefit is that our model (4.27) admits prior specification of a bipolar end state. Previous adaptive control models in [29] involve a different control mechanism and find (numerically) the optimal control to drive the graph to a consensus state (3.23). However, the limitation noted by the authors is that there is no mechanism to steer the graph towards a desired bipolar state. This limitation is overcome here, and with reasonably low values of the control parameter β - the subject of investigation in the following section.

4.2.1 Test for β

We now outline a numerical test to determine which values of β result in convergence to the desired state X^*. To quantify how close the final state $X(t_c)$ is to the desired state X^*, it is useful for our purposes to define a similarity measure. For two matrices A and B, the metric $S \in [0, 1]$ is defined as

$$S(A, B) = 1 - \frac{1}{2n^2 R}||A - B||_F, \tag{4.29}$$

where $||\cdot||_F$ denotes the Frobenius matrix norm. We construct this with the properties $S(A, A) = 1$ and $S(A, -A) = 0$.

For each test run, we use a symmetric standard Gaussian initial condition and a randomly initialised target state, $v_i = \sqrt{R}(2B - 1)$, $B \sim \mathcal{B}(1/2)$, where $\mathcal{B}$ is the Bernoulli distribution. The convergence with respect to the similarity measure

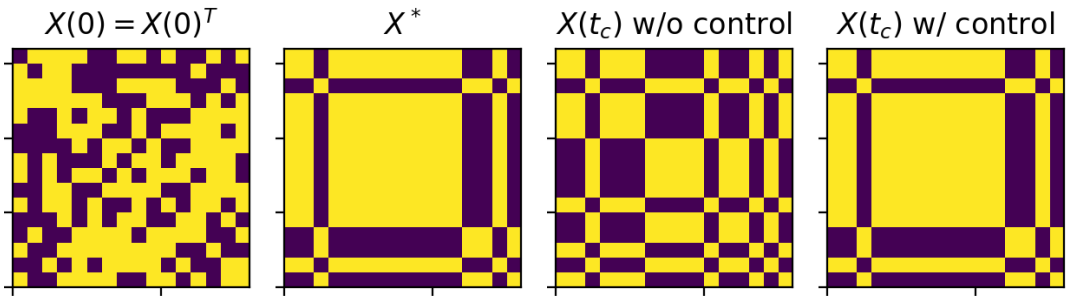

Figure 4.5: Plots of the initial condition, desired state defined by random target vector $X^* = \mathbf{v}\mathbf{v}^T$, and end states without and with control. Clearly the controlled end-state matches X^*. The cut-off time $t_c > t^*$ is chosen arbitrarily once the dynamics reach a steady state. The associated dynamics are shown in Figure 4.6. $R = 10$, $\beta = 0.025$, $n = 16$.

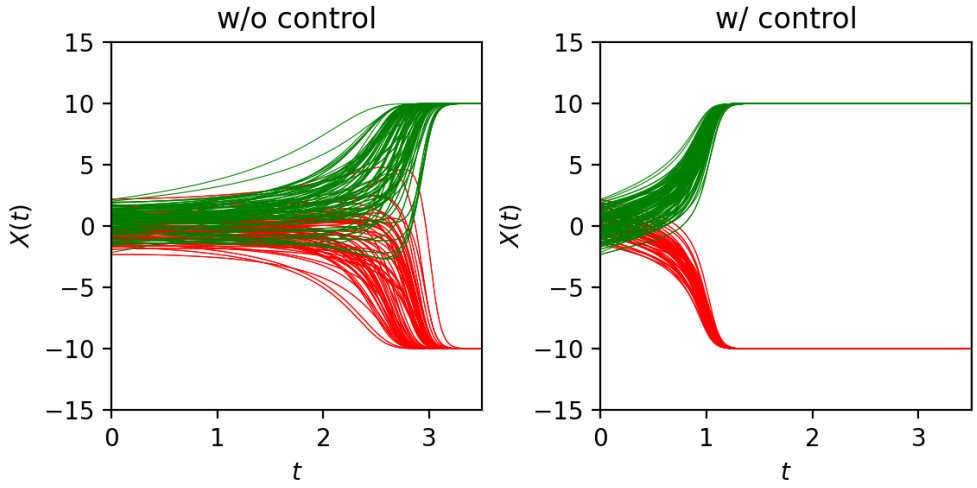

Figure 4.6: Controlled and uncontrolled dynamics for a random desired state. $R = 10$, $\beta = 0.025$, $n = 16$.

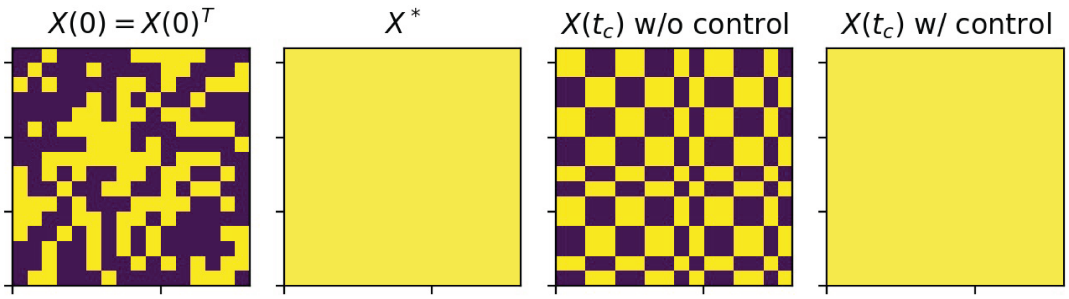

Figure 4.7: Plots of the initial condition, desired consensus state X^*, and end states without and with control. The steady-state of the controlled model is consensus, again matching X^*. The associated dynamics are shown in Figure 4.8. $R = 10$, $\beta = 0.025$, $n = 16$.

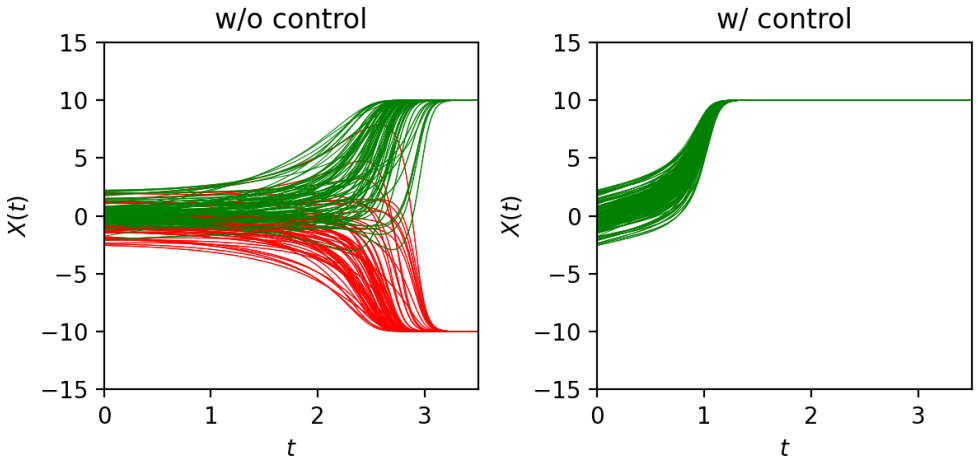

Figure 4.8: Controlled and uncontrolled dynamics for a desired consensus state. $R = 10$, $\beta = 0.025$, $n = 16$.

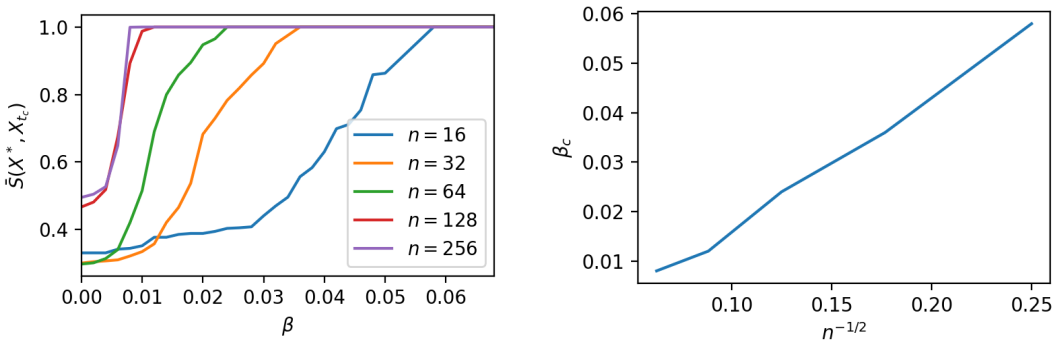

Figure 4.9: Average similarity $\bar{S}$ between the controlled end-state $X_{t_c} = X(t_c)$ and the desired state X^* with respect to the static control variable β, averaged over 10 test runs with $X_0 \overset{iid}{\sim} \mathcal{N}(0,1)$ (left). The critical control value β_c for convergence is plotted against $n^{-1/2}$. $R = 10$.

is shown in Figure 4.9 for various values of n. What we note from Figure 4.9 is the relatively low values of β for which the desired state is reached, for example $\beta \geq 0.035$ for a random graph of size $n = 32$.

We find a dependence on n for $n \lesssim 256$, which is a result of the random initial conditions used, $X_0 \sim \mathcal{N}(0,1)$. At $t = 0$, the sum $\sum_{k \in V} X_{ik} X_{kj}$ is normally distributed and centred on zero by the Central Limit Theorem, hence the deviation of the sum from zero decreases with $\sqrt{n}$, in which cases the relative influence of the control is greater. Hence for small n, we expect the influence of the graph size on the critical control value for which the desired state is reached, β_c, to be proportional to $1/\sqrt{n}$. This is illustrated in Figure 4.9.

4.2.2 Stability of the control model

We now show that the condition on β for the stability of balanced fixed points, $X^* \in \mathcal{B}$, is $\beta < R/(R+2)$. We define entries of the control model (4.27) as $\dot{X}_{ij} = D_{ij}(X; R, \mathbf{v}) = D_{ij}$ and proceed as in Section 4.1.3. In the case where X_{ij} matches the desired fixed point X^*_{ij}, the control has no effect, and the corresponding diagonal entry in the Jacobian is $-2R(1-\beta)$, stable as before. When such states do not match, then $X^*_{ij} - X_{ij} = \mp 2R$, and the corresponding entry on the

diagonal of the Jacobian is

$$\left.\frac{\partial D_{ij}}{\partial X_{ij}}\right|_{X^*_{ij}=\pm R} = -2R(1-\beta)+4\beta. \tag{4.30}$$

This is less than zero for all i, j provided $\beta < R/(R+2)$, for which the balanced fixed point is stable. This is a mild condition given our numerical results above, typically requiring $\beta \sim 10^{-2}$ for the end state to match a random desired state.

We now define our prescribed rank-one matrix $X^* = \mathbf{v}\mathbf{v}^T$ as a *diplomatic target*, which in the context of the initial value problem serves to constantly nudge opinions or relations towards a specified state. Applying this to the case study of countries leading to WWI in the paper by Antal *et al.* [24] and also in comparing it to the model proposed by Marvel *et al.* [19] on a dataset harvested from Zachary's karate club study [34], we show in both cases that this model correctly classifies all parties for reasonably low values of the control parameter β.

4.2.3 Case study 1: Alliances in World War I

We apply the models to the example of alliances and enmity between nations in the period leading up to WWI shown in Figure 2.2. This is given as an empirical example of international relations tending toward socially balanced states in Antal *et al.* [24], shown in Figure 2.2, but it is not used in the analysis of their model. We use each snapshot up to 1904 as an initial condition, run the control model using the 1907 Allied and Axis alignments as the diplomatic target, investigating how it performs versus the uncontrolled model with saturation (4.6) as both models are initialised closer to the outbreak. Results are shown in Figure 4.10.

We observe that the controlled model leads the graph to the desired state in every case. The uncontrolled model only achieves the correct classification for the 1904 initial configuration. Otherwise, the uncontrolled model typically misclassifies one country. An interesting point of note is that the non-control model also fails to elicit any relationships for Italy in the first instance, where Italy is disconnected from the graph. The control model successfully inserts Italy into the final state, however, which points to its use in modelling the growth of *initially disconnected* graphs, where vertices that are disconnected under the original model would otherwise remain disconnected.

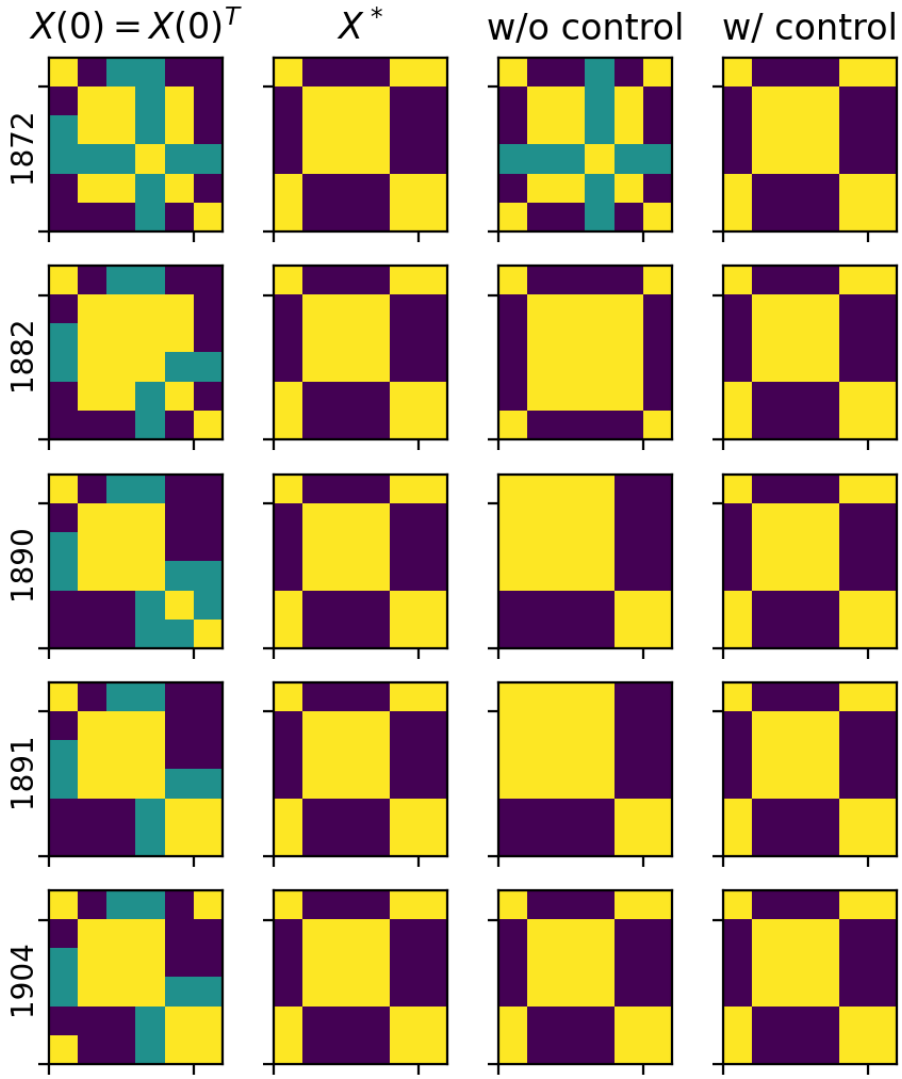

Figure 4.10: Controlled dynamics of positive (yellow), neutral (green), and negative (purple) relations between nations preceding WWI. Initial states (far-left column) are obtained for different years from [24], and the diplomatic target for the control model is given by the 1907 state of Allied and Axis forces (mid-left). End states predicted by the original model with saturation (4.6) (mid-right) versus the control model (4.27) (far-right).

initial year	β
1872	0.119
1882	0.122
1890	0.016
1891	0.029
1904	0.000

Table 4.1: Minimum values of β for which every country is successfully classified to three decimal places, given initial data at the years specified.

The minimum values of the control parameter for which the model correctly classifies every nation is given in Table 4.1. Referring to Figure 2.2, we argue that in the first two instances, a larger value of β is required to achieve the desired state because there are fewer edges present in the graph, i.e. the initial data is more sparse, and edges present involve positive relations between Russia and both Austria-Hungary and Germany, an alliance that does not persist. As the year from which the model is initialised becomes closer to the outbreak in 1914, we find that values of β one order of magnitude lower are required to reach the desired state. From 1904, the original model correctly classifies each party. The difficulty in predicting the final state from earlier years of course reflects the inherently stochastic nature of social relations, but it proves reasonably effective when initialising from later years, in which only low values of β are required to reach the actual state.

4.2.4 Case study 2: Zachary's karate club

Zachary's karate club study [34] is a well-known example in network theory, concerning the fission of small groups into two opposing factions. The study follows the relationships between 34 members as a club split in two due to instructor wage disagreements. The benefit of the supplied dataset is that it provides information on the frequency of social interaction between individuals shortly before the fission and details of which faction-club individuals joined afterwards.

In the study, the frequency of interaction is argued to be linearly dependent on the strength of relationships and quantified on a scale of discrete values in the range $[0, 8]$. For our investigation, this range is scaled to $[-1, 1]$. Data for the target state $X^* = \mathbf{v}\mathbf{v}^T$ and initial state $X_0 \in \mathbb{R}^{34\times 34}$ are harvested from the paper [34].

Numerical solutions to the saturating model without control (4.6) and the static control system (4.27) for the dynamics and final-state are shown in Figures 4.11 and 4.12 respectively. The desired state is achieved for $\beta = 0.009$.

A similar study is performed by Marvel *et al.* in [19] for the unbounded dynamics $\dot{X} = X^2$, as in (3.2). The classification of the end states is found here to be the same for the analogous model including saturation (for $R = 10$). These models at best misclassify one individual in the bipolar steady state. However, by adding a small term that nudges the system towards the desired state as introduced here in (4.27), the system correctly classifies all members in the final state.

In this section, we presented a novel adaptive control scheme to drive the graph to any prescribed balanced state. This improves on the limitations of previous models [29], which are only able to steer the graph to consensus. We derive a stability criterion for our control model at balanced states, $\beta < R/(R+2)$, considered mild given that the requirement to bring a random initial state to a target is typically on the order of $\beta \sim 10^{-2}$, found numerically.

The two case studies presented show that a specific bipolar state may be achieved for low values of the control parameter β. In both cases, we prescribed the desired state X^* based on the known final associations of vertices in the graph. In reality, such states are not known *a priori*. However, the control parameter may be tuned such that the final balanced state accounts for the state vector $\mathbf{v}$, but is not determined by it. Hence, $\mathbf{v}$ may be used to encode other non-deterministic influences, such as expert analysis, histories of relations, known political sentiment, or knowledge from data mining. In such cases, β may be used to quantify the modeller's trust in the knowledge source. This control model may also be applied to connect initially disconnected graphs, which as we illustrated would otherwise stay disconnected in uncontrolled settings.

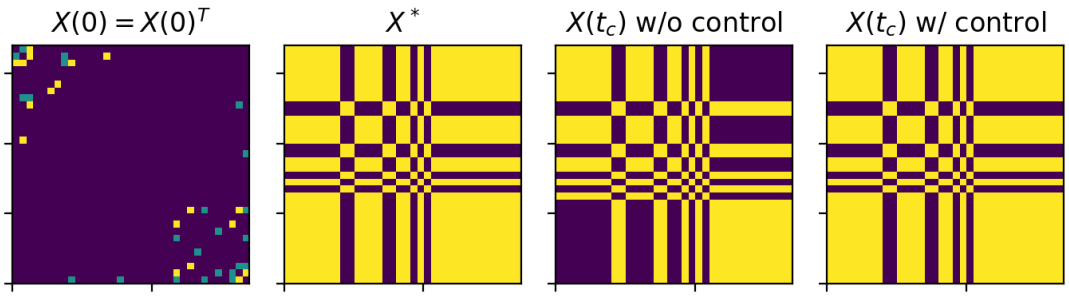

Figure 4.11: The initial state of relations between club members (far left), followed by the actual balanced distribution of members following the fission of the club (mid-left). The steady-state without control (mid-right) misclassifies at least one individual [19], depending on the linear map used for the initial conditions. The controlled steady-state (far right) matches the actual result. This is achieved for a relatively low value of the control parameter, with a lower bound of $\beta = 0.009$ to three decimal places.

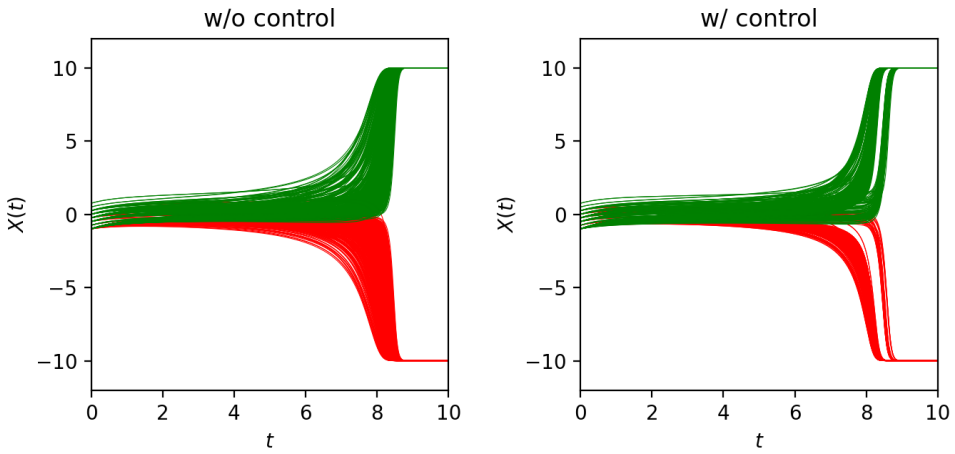

Figure 4.12: Associated dynamics of relations initialised with data from Zachary's karate club study. Here $R = 10$, $n = 34$, $\beta = 0.009$.

4.3 Multiplex graphs

Aside from adding a control mechanism, another interesting extension of the dynamics is to couple (linearly) the dynamics of multiple layers of a multiplex graph. For unbounded models, the application to multilayer graphs is not particularly interesting. Once one layer blows up, it dominates the dynamics of the other layers for all $\alpha \in (0, 1]$. The result, which is verified computationally, is that the final state of every layer is identical. However, this is not the case when the model with saturation (4.6) is generalised to a multiplex topology. For a graph with two layers, $L = 2$,

$$\begin{aligned} \dot{X}_1 &= (1-\alpha)M(X_1) + \alpha M(X_2), \quad X_1(0) = X_{0(1)}, \\ \dot{X}_2 &= (1-\alpha)M(X_2) + \alpha M(X_1), \quad X_2(0) = X_{0(2)}, \end{aligned} \tag{4.31}$$

there is a critical value of the coupling parameter α, above which both layers tend to the same balanced state and below which the layers tend to different states. The dynamics and end-states are illustrated for a range of α in Figure 4.13. Again using the similarity measure, $S(X_1, X_2)$, the equivalence of the final states for $\alpha \gtrsim 0.35$ given random initial conditions is shown in Figure 4.14. We also provide a local analysis for the nine fixed points of the associated reduced system in $\mathbb{R}^2$ when considering constant initial conditions, $X_1(0), X_2(0) \in \mathcal{C}$. This is outlined in Appendix A. As we characterise the relevant fixed points for the full system (4.31), we do not include the analysis of the reduced system here.

4.3.1 Stability of utopian and dystopian states

We have already proven the stability of the system around the two fixed points $X^* = \pm R\,\mathbf{1}_{n\times n}$ for a single layer, $L = 1$, in Section 4.1.3. This provides a basis for consideration of the multiplex case. In the $L = 2$ multiplex case, it is again helpful to consider the elementwise form of (4.31),

$$\begin{aligned} \dot{X}_{ij(1)} &= (1-\alpha)\frac{1}{n}\left(1 - \frac{X_{ij(1)}^2}{R^2}\right)\sum_{k\in V} X_{ik(1)}X_{kj(1)} + \alpha\frac{1}{n}\left(1 - \frac{X_{ij(2)}^2}{R^2}\right)\sum_{k\in V} X_{ik(2)}X_{kj(2)}, \\ \dot{X}_{ij(2)} &= (1-\alpha)\frac{1}{n}\left(1 - \frac{X_{ij(2)}^2}{R^2}\right)\sum_{k\in V} X_{ik(2)}X_{kj(2)} + \alpha\frac{1}{n}\left(1 - \frac{X_{ij(1)}^2}{R^2}\right)\sum_{k\in V} X_{ik(1)}X_{kj(1)}. \end{aligned} \tag{4.32}$$

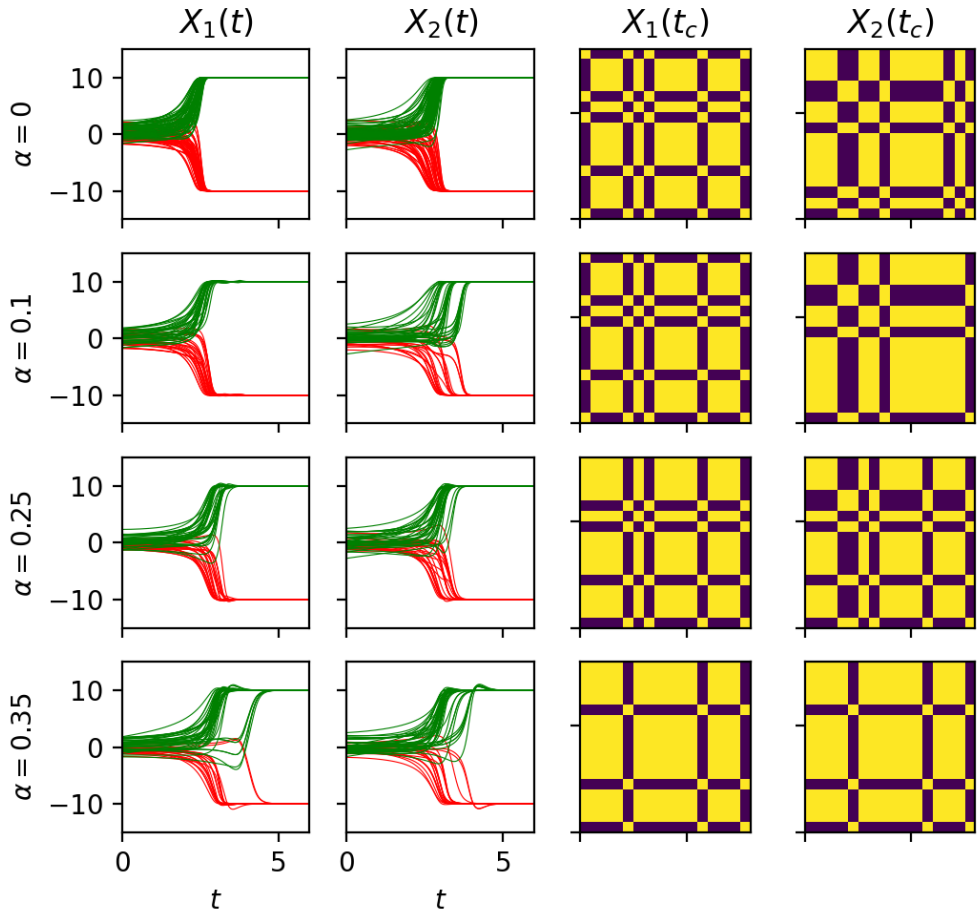

Figure 4.13: Dynamics and end-states of two layers, with respect to the coupling parameter α. Both layers tend to the same state for $\alpha = 0.35$, agreeing with the numerical test in Figure 4.14. At higher values of α the dynamics are more strongly coupled and begin to show oscillatory behaviour, overshooting $\pm R$. Both initial conditions are iid and drawn from a standard normal distribution $\mathcal{N}(0, 1)$. $R = 10$ and $n = 16$.

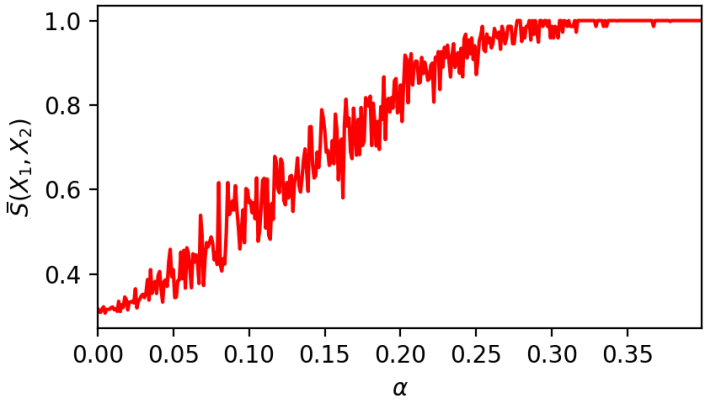

Figure 4.14: Equivalence of multiplex end states, averaged over 25 tests, with respect to α, quantified by the similarity measure (4.29). $R = 10$, $n = 16$.

We proceed as in Section 4.1.3. Vectorising the entire system and taking the partial derivative with respect to $(\mathcal{X}_{(1)}, \mathcal{X}_{(2)}) \in \mathbb{R}^{2K}$ results in the Jacobian $J \in \mathbb{R}^{2K \times 2K}$. The entries are evaluated at the fixed points $X^*_{(1)} = X^*_{(2)} = \pm R\,\mathbf{1}_{n\times n}$, resulting in the following block Jacobian matrix, denoted $J_\pm$ for convenience,

$$J_\pm = \mp 2R \begin{pmatrix} (1-\alpha)I_K & \alpha I_K \\ \alpha I_K & (1-\alpha)I_K \end{pmatrix}. \tag{4.33}$$

We use the following identity for a block matrix [35],

$$\begin{vmatrix} A & B \\ C & D \end{vmatrix} = |A||D - CA^{-1}B|. \tag{4.34}$$

Note that the block A must be invertible, hence we assert $\lambda \neq \mp 2R(1-\alpha)$, and solve the characteristic polynomial for the eigenvalues,

$$|J_\pm - \lambda I_{2K}| = 0, \tag{4.35}$$

which yields the spectrum of $J_\pm$, given by,

$$\lambda \in \{\mp 2R(1-2\alpha),\ \mp 2R\}, \quad \alpha \neq 0. \tag{4.36}$$

The value $\alpha = 0$ is neglected as it is the only case where $\lambda \neq \mp 2R(1-\alpha)$ is not satisfied. Hence, for $0 < \alpha < 1/2$, the fixed point $X^*_{(1)} = X^*_{(2)} = R\,\mathbf{1}_{n\times n}$ is stable and $X^*_{(1)} = X^*_{(2)} = -R\,\mathbf{1}_{n\times n}$ is unstable. A bifurcation occurs at $\alpha = 1/2$ and neither fixed point is stable for $\alpha > 1/2$.

4.3.2 Stability of all balanced fixed points

We now characterise the stability of all of the balanced fixed points of the system, showing that they are stable for $a < 1/2$. In such cases we show that it is not necessary for each graph to be in the same balanced state, i.e. $X_{ij(1)}$ can belong to a different faction than $X_{ij(2)}$, provided each layer of the fixed point $(X^*_{(1)}, X^*_{(2)})$ is balanced.

As in section 4.1.3, we are interested in inferring the sign of the sums contained in (4.32), which dictate the signs of the corresponding entries in the Jacobian. We invoke our previous observation that in balanced graphs this sum equals nR^2 if i and j belong to the same faction and $-nR^2$ if they belong to different factions (i.e. $X_{ij} = R$ or $X_{ij} = -R$ at the fixed point respectively). This is now a function of the layer, l, hence we define the observation using a function $\phi_{(l)}(i,j)$ to represent the sign of $X_{ij(l)}$ so we can express the summation as

$$\sum_{k\in V} X_{ik(l)}X_{kj(l)} = nR^2\phi_{(l)}(i,j), \quad \phi_{(l)}(i,j) = \begin{cases} +1, & X_{ij(l)} > 0 \\ -1, & X_{ij(l)} < 0 \end{cases}. \tag{4.37}$$

Proceeding as before, noting that only the entries on the diagonal $(p,q) = (i,j)$ of each block in the Jacobian are nonzero, the diagonal entries are given by

$$\frac{\partial M_{ij(1)}}{\partial X_{ij(1)}}\Big|_{X_{ij}=\pm R} = -2R(1-\alpha), \tag{4.38a}$$

$$\frac{\partial M_{ij(1)}}{\partial X_{ij(2)}}\Big|_{X_{ij}=\pm R} = \mp R\phi_2(i,j) = -2R\alpha\phi_{(1)}(i,j)\phi_{(2)}(i,j), \tag{4.38b}$$

$$\frac{\partial M_{ij(2)}}{\partial X_{ij(1)}}\Big|_{X_{ij}=\pm R} = \mp R\phi_1(i,j) = -2R\alpha\phi_{(2)}(i,j)\phi_{(1)}(i,j), \tag{4.38c}$$

$$\frac{\partial M_{ij(2)}}{\partial X_{ij(2)}}\Big|_{X_{ij}=\pm R} = -2R(1-\alpha). \tag{4.38d}$$

Note in (4.38b) and (4.38c) the additional ϕ accounts for the sign of the entry X_{ij} and hence the associated $\mp$ sign, allowing us to express the Jacobian as

$$J = -2R\begin{pmatrix} (1-\alpha)I_K & \alpha\Phi_{(1)}\Phi_{(2)} \\ \alpha\Phi_{(1)}\Phi_{(2)} & (1-\alpha)I_K. \end{pmatrix}, \tag{4.39}$$

In essence the matrix $\Phi_{(l)} \in \{-1,0,1\}^{K\times K}$ encodes the sign of each vertex $(i,j) \in T$ along the diagonal in a given layer,

$$\Phi_{(l)} = \mathrm{diag}(\phi_{(l)}(i,j)) = \mathrm{diag}(\mathrm{sign}(\mathcal{X}_{(l)})), \quad l = 1,2. \tag{4.40}$$

Again we use the identity (4.34) to calculate the characteristic polynomial for $\lambda \neq -2R(1-\alpha)$. Dropping the factor of $-2R$, the sign matrices cancel yielding,

$$\begin{vmatrix} (1-\alpha-\lambda)I_K & \alpha\Phi_{(1)}\Phi_{(2)} \\ \alpha\Phi_{(1)}\Phi_{(2)} & (1-\alpha-\lambda)I_K \end{vmatrix} = \lambda^2 - 2(1-\alpha)\lambda + (1-2\alpha) = 0 \tag{4.41}$$

Leading to the eigenvalues (on inclusion of the factor of $-2R$),

$$\lambda \in \{-2R(1-2\alpha), -2R\}, \quad \alpha \neq 0. \tag{4.42}$$

Hence for $0 < \alpha < 1/2$ if both layers constituting a fixed point are balanced, the fixed point is stable. It is not necessary that the layers are balanced identically, i.e. that $X^*_{(1)} \equiv X^*_{(2)}$, as the sign difference cancels in evaluating the eigenvalues. This result is consistent with our previous proof of the stability of the utopian state. There is a bifurcation at $\alpha = 1/2$, above which the balanced fixed points are not stable.

In our setting, the layers of a multiplex graph may represent different planes of social interaction between entities, for example individuals may differ in their political orientation depending on the topic of debate, or the state of affairs between nations may differ depending on the subject, e.g. trade, migration, peace treaties, etc. We would expect the state of one layer to be influenced by that of others, but not more so than that of itself. Hence, we argue, the bifurcation at $\alpha = 1/2$ and the associated instabilities of balanced states above this value are not relevant to our context, although it may prove an interesting topic for further work.

In this section, we discussed the application of bounded dynamics to multiplex graphs. In the $L = 2$ case, we show that the dynamics are stable at fixed points provided each layer is in a state of balance, and that it is not necessary for layers to be in the same state of balance in order for the fixed point to be stable. Indeed for low values of α, the dynamics of both layers tend towards different balanced states. From a social perspective, this accounts for cognitive dissonance: individuals may prescribe to different ideologies depending on the topic, or countries might choose different sides depending on the diplomatic context. We can also increase the coupling between layers such both do tend towards the same balanced state, our numerical results showing that this occurs for $\alpha \gtrsim 0.3$.

Chapter 5

Conclusion

In this dissertation, we provided an overview of the socio-psychological origins of balance in social networks and its subsequent formalism within graph theory. We then motivated the use of models in continuous time to drive an initially imbalanced graph to a state of balance. This involved first exploring existing models which typically contain finite-time singularities, reflecting how once a graph reaches a balanced state, opinions diverge. This is however unrealistic, hence we focused on bounded models, parameterised with a saturation value R. We used a model which includes reflexive relationships and studied the stability of the associated fixed points and convergence to a balanced state. To our knowledge, this marked the beginning of the novel contributions of the dissertation. We outlined two model extensions. The first is a static control model, which serves to nudge the system onto an orbit that reaches a desired balanced state, X^*. This model was applied to two case studies: the alliance and opposition between nations in the years preceding WWI; and group fission in a well-known karate club study. In both cases, the model successfully classified the members of each party in the final state. The second extension investigated coupled dynamics between layers of multiplex graphs. We investigated the stability of the system and the values of the coupling parameter α for which the layers tend to identical balanced states. For $\alpha < 1/2$ we found that the layers can tend to different balanced steady states and be stable under the associated dynamics, and we interpreted this in the context of social networks.

5.1 Limitations

There are several limitations to the general framework presented in this dissertation. First, there are limitations to the Heider balance model and the associated dynamics, in that it does not account for the inherent unpredictability of relations between social individuals. We see this in the difficulty the control model has in predicting the Russia-Hungary lapse in the WWI case study. Heider balance theory also only accounts for 'bipartisan fission', applicable to settings where a group undergoes fission into maximally two factions. This is sufficient in applications such as Zachary's karate club study, but is not always observed in social settings where human relations are typically stochastic and less consistent [36]. Other paradigms admit notions of weak structural balance - "Machiavellian" configurations [37] in which a triad with three negative edges is considered balanced, allowing for more than two factions to constitute a balanced graph.

In the multiplex model, if one layer is initialised with negative relations, it may force both layers to a consensus state. An example of this is plotted in Figure A.7. Applied to social settings, this is an artefact of the dynamics that seems unrealistic and should be investigated in further work.

5.2 Further work

We finish by outlining a few natural progressions from the current work. For the control model, it would be interesting to investigate the performance of this model without a prior knowledge of the desired state. Thus a key challenge would be how to prescribe the diplomatic target vector. Some approaches we suggested are data mining or expert analysis, the control parameter β quantifying the modeller's trust in the source. Another avenue of exploration is optimal control, where a cost functional may be defined for a dynamic control parameter varying in time, $\beta(t)$. A numerical example is outlined in [29]. Another option is to data-drive the control parameter to track the dynamics of real social interactions.

Another feasible extension would be to consider $L > 2$ layers in a richer multiplex graph topology, investigating the interplay between interlayer dynamics and intralayer dynamics.

It would be interesting to adopt a general stochastic model, reflecting the nature of social interactions. A simple extension would be to include a multiplicative stochastic variable, for example,

$$\mathrm{d}X = X^2\,\mathrm{d}t + \sqrt{\sigma}X^2\,\mathrm{d}W,$$

where W is a Weiner process. This approach would be in the spirit of stochastic variations of flocking models, e.g. the stochastic Cucker-Smale model, which is briefly suggested as an extension to the control system in Wongkaew [29]. Such a model could be used to investigate how robust the dynamics or control are to noise.

Appendix A

Reduced multiplex dynamics

To investigate the stability of the fixed points of the problem (4.31), we consider simplified dynamics for $n = 1$. For $x_1, x_2 \in \mathbb{R}$ and $R = 1$, we have

$$\begin{aligned} \dot{x}_1 &= (1-\alpha)(1-x_1^2)x_1^2 + \alpha(1-x_2^2)x_2^2 \\ \dot{x}_2 &= (1-\alpha)(1-x_2^2)x_2^2 + \alpha(1-x_1^2)x_1^2. \end{aligned} \tag{A.1}$$

Letting $\mathbf{x} = (x_1, x_2)^T$, the associated set of nine fixed points for the system are

$$\mathbf{x}^* = \{(0,0), (\pm 1, 0), (0, \pm 1), (\pm 1, \pm 1)\}.$$

Each of these fixed points are in the domain $\Omega \equiv [-1, 1] \times [-1, 1]$, the extent determined by $R = 1$. The Jacobian, taken with respect to $\mathbf{x}$, is given by

$$J(\mathbf{x}; \alpha) = 2 \begin{pmatrix} (1-\alpha)(1-2x_1^2)x_1 & \alpha(1-2x_2)x_2 \\ \alpha(1-2x_1)x_1 & (1-\alpha)(1-2x_2^2)x_2 \end{pmatrix}. \tag{A.2}$$

The phase planes of the $n = 1$ system are simulated for a range of values of α in Figure A.1. We refer the reader to Appendix B for numerical results of the local stability around each fixed point.

The eigenvalues and eigenvectors of (A.2) for each of the nine fixed points are given in Table A.1. The stability of *hyperbolic fixed points*, which satisfy

$$\mathcal{R}(\lambda) \neq 0, \ \forall \, \lambda \in \mathrm{Spec}(J(\mathbf{x}^*; \alpha)),$$

is completely determined by linearisation of the field around each fixed point [38]. The set of hyperbolic fixed points is given by $\mathcal{H}$. The stability of $\mathbf{x}^* \in \mathcal{H}$ is hence given by the following theorem, from [39].

$\mathbf{x}^*$	$J(\mathbf{x}^*;\alpha)$	λ
(0,0)	$\begin{pmatrix} 0 & 0 \\ 0 & 0 \end{pmatrix}$	$\{0, 0\}$
(1,0)	$2\begin{pmatrix} -(1-\alpha) & 0 \\ -\alpha & 0 \end{pmatrix}$	$\{0, -2(1-\alpha)\}$
(-1,0)	$2\begin{pmatrix} (1-\alpha) & 0 \\ \alpha & 0 \end{pmatrix}$	$\{0, 2(1-\alpha)\}$
(0,1)	$2\begin{pmatrix} 0 & -\alpha \\ 0 & -(1-\alpha) \end{pmatrix}$	$\{0, -2(1-\alpha)\}$
(0,-1)	$2\begin{pmatrix} 0 & \alpha \\ 0 & (1-\alpha) \end{pmatrix}$	$\{0, 2(1-\alpha)\}$
(-1,1)	$2\begin{pmatrix} 1-\alpha & -\alpha \\ \alpha & -(1-\alpha) \end{pmatrix}$	$\{-2\sqrt{1-2\alpha}, 2\sqrt{1-2\alpha}\}$
(1,-1)	$2\begin{pmatrix} -(1-\alpha) & \alpha \\ -\alpha & 1-\alpha \end{pmatrix}$	$\{-2\sqrt{1-2\alpha}, 2\sqrt{1-2\alpha}\}$
(-1,-1)	$2\begin{pmatrix} 1-\alpha & \alpha \\ \alpha & 1-\alpha \end{pmatrix}$	$\{2(1-2\alpha), 2\}$
(1,1)	$2\begin{pmatrix} -(1-\alpha) & -\alpha \\ -\alpha & -(1-\alpha) \end{pmatrix}$	$\{-2, -2(1-2\alpha)\}$

Table A.1: Eigenvalues of the Jacobian evaluated at the nine fixed points of the system (A.1). The last four rows, corresponding to the fixed points at the corners of Ω, undergo a bifurcation at $\alpha = 1/2$.

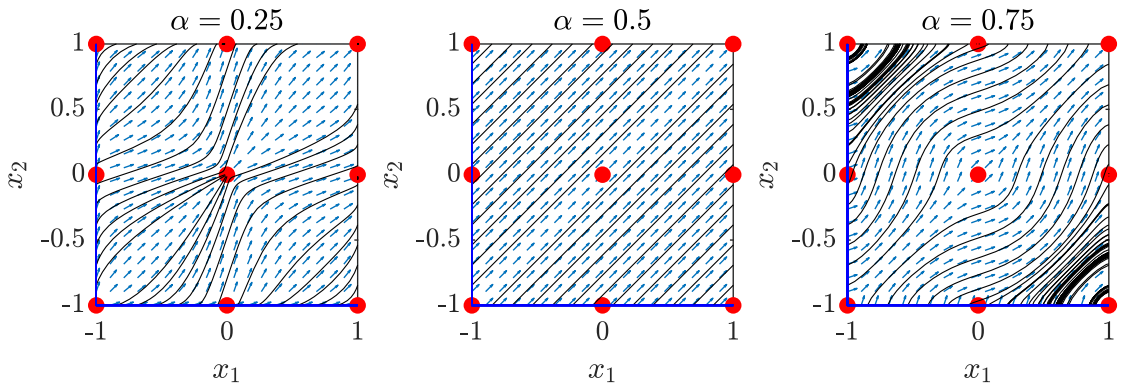

Figure A.1: Phase portrait of the system (A.3), with fixed points shown in red. A bifurcation occurs at $\alpha = 1/2$. Phase lines are initialised along the blue line, with trajectories shown in black.

Theorem 6. *For all* $\mathbf{x}^* \in \mathcal{H}$*, if, for a given* α*,* $\mathcal{R}(\lambda) < 0$*,* $\forall\, \lambda \in Spec(J(\mathbf{x}^*; \alpha))$*, then* $\mathbf{x}^*$ *is asymptotically stable. Otherwise there exists a* λ *such that* $\mathcal{R}(\lambda) > 0$*,* $\lambda \in Spec(J(\mathbf{x}^*; \alpha))$*, and* $\mathbf{x}^*$ *is unstable.*

From Table A.1, for $\alpha < 1/2$, there are four hyperbolic fixed points

$$\mathcal{H} = \{(\pm 1, \pm 1)\},$$

of which only $\mathbf{x}^* = (1, 1)$ is stable. The other three contain an unstable linear subspace (which is tangent to a one-dimensional unstable manifold) hence, by Theorem 6, they are unstable fixed points. At $\alpha = 1/2$ a bifurcation occurs at every fixed point in $\mathcal{H}$. At the equilibria $\pm(1, 1)$, the eigenvalues pass through zero, a bifurcation being implied by a change in stability of the associated linear subspaces. A more complex bifurcation occurs at $\pm(1, -1)$. If viewed in the complex plane, the eigenvalues approach each other on the real line, collide, and become complex conjugate. Such a bifurcation is known as a saddle-centre bifurcation [40]. For $\alpha \geq 1/2$ the set of hyperbolic fixed points is empty, $\mathcal{H} = \varnothing$.

A.1 Classification of fixed points with singular Jacobian

In the case of the five non-hyperbolic fixed points for $\alpha < 1/2$, or seven for $\alpha > 1/2$, the Jacobian at each fixed point has at least one zero eigenvalue with an associated

centre linear subspace, tangent to a centre manifold, W^c [38]. Both $(-1, 0)$ and $(0, -1)$ have an unstable subspace for $\alpha \in [0, 1)$[1], thus we can conclude in such cases that these equilibria are unstable. In the case of one zero eigenvalue and one negative eigenvalue, the local dynamics around $x^* \notin \mathcal{H}$ are governed by the reduced dynamics on the centre manifold.

For the equilibria $(1, 0)$ and $(0, 1)$ we can analyse the dynamics on the centre manifold. This in essence involves projecting the local dynamics onto the centre manifold, reducing the number of state variables of the system, then extending the centre manifold by one dimension to include the bifurcation parameter α [41]. We note that the system dynamics are symmetric about $x_1 = x_2$, thus it is sufficient to characterise the stability of one of the above points. We leave this characterisation to further work, if necessary.

A.1.1 Degenerate centre

In the case of the quadratic system (A.1) with degenerate linear terms, such as $(0, 0)$, one approach is to investigate the dynamics via Normal Form analysis, in which non-resonant terms close to a fixed point are removed by a near-identity transformation [41]. However, a more straightforward analysis is available if we take advantage of the symmetry of the problem. This is the approach taken below.

We may classify the local stability of the point $(0, 0)$ by noting it lies on the line $x_1 = x_2$, which is an invariant set under the flow. Hence we may reduce the dimension of the problem to $\dot{x} = f(x) \in \mathbb{R}$, defined as

$$\dot{x} = f(x) = x^2(1 - x^2), \tag{A.3}$$

and study the dynamics around the fixed points $x^* = \{-1, 0, 1\}$. The plot of (A.3) is shown in Figure A.2. In the one dimensional case, the Jacobian is identical to the derivative, $D_x f(x) = 2x(1 - 2x^2)$, from which we can see that $D_x f(-1) > 0$ and $D_x f(1) < 0$ hence the point $x^* = -1$ is unstable and the point $x^* = 1$ is stable along the invariant $x_1 = x_2$, in agreement with our earlier analysis. Although $D_x f(0) = 0$, we can observe the behaviour of $f(x)$ in Figure A.2 around $x^* = 0$ to determine the stability of the fixed point. As $D_x f(\epsilon) > 0$ for $\epsilon \ll 1$, we deduce that $x^* = 0$ is unstable and hence, by symmetry, $\mathbf{x}^* = (0, 0)$ is unstable $\forall\, \alpha$.

[1] We address the local stability for $\alpha = 1$ in later sections.

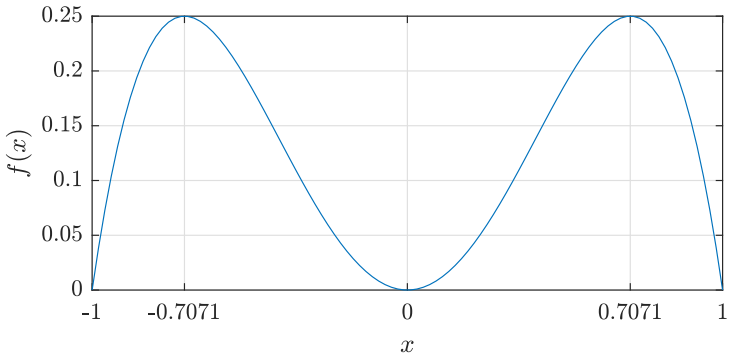

Figure A.2: Plot of the reduced system (A.3).

A.1.2 Saddle-centre bifurcation

For the points $\pm(1,-1)$ eigenvalues of the Jacobian are given by

$$\lambda_{1,2} = \pm 2\sqrt{1-2\alpha}, \quad \alpha \in [0,1], \tag{A.4}$$

hence for $\alpha < 1/2$, $\lambda_{1,2}$ are real, non-zero, and distinct. As one of them is positive, these equilibria are unstable in this range of α, as proven earlier. Both eigenvalues pass through zero at $\alpha = 1/2$ and become complex conjugate for $\alpha > 1/2$, suggesting the presence of periodic behaviour, however drawing conclusions of the stability of such is non-trivial. Numerical simulations of the global behaviour are shown in Figure A.1, with a bifurcation at $\alpha = 1/2$. Numerical solutions indicate the presence of limit cycles for $\alpha = 1$. Refer to Figure B.1 in Appendix B for a local phase portrait around $(1,-1)$.

Another option for identifying the stability of such points is to find a first integral for the system, within level sets of which orbits are confined. However, using Mathematica we found that no first integral polynomial exists in general, up to degree 20. This is not the case when $\alpha = \{0,1\}$ however, which we explore in the following sections.

A.2 First integral for $\alpha = 1$

Representing the reduced system as

$$\begin{aligned} \dot{x}_1 &= (1-\alpha)x_1^2(1-x_1^2) + \alpha x_2^2(1-x_2^2), \\ \dot{x}_2 &= (1-\alpha)x_2^2(1-x_2^2) + \alpha x_1^2(1-x_1^2), \end{aligned} \tag{A.5}$$

in the case where $\alpha = 1$ we can find a first integral,

$$\begin{aligned} \frac{\mathrm{d}x_1}{\mathrm{d}x_2} &= \frac{f(x_2)}{f(x_1)} \\ \int f(x_1)\,\mathrm{d}x_1 &= \int f(x_2)\,\mathrm{d}x_2 + c \\ \frac{1}{3}x_1^3 - \frac{1}{5}x_1^5 &= \frac{1}{3}x_2^3 - \frac{1}{5}x_2^5 + c \end{aligned} \tag{A.6}$$

Hence we can plot level sets of the function

$$V(x_1, x_2) = \frac{1}{3}x_1^3 - \frac{1}{5}x_1^5 - \frac{1}{3}x_2^3 + \frac{1}{5}x_2^5, \tag{A.7}$$

and compare them to the numerical phase portrait, as in Figure A.3.

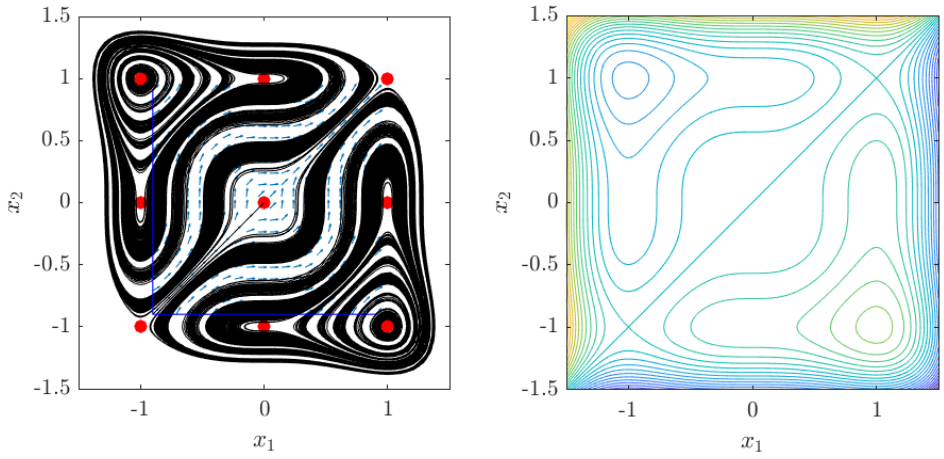

Figure A.3: Numerical phase portrait of the system (A.3) with $\alpha = 1$ (left) and level sets of the function (A.7) (right).

Every orbit is contained in some level set of $V(x_1, x_2)$, defining an invariant of the flow of (A.1). The level sets $V = \{0, \pm\frac{2}{15}, \pm\frac{4}{15}\}$ contain fixed points, while all other level sets containing points in the domain $\Omega = [-1, 1] \times [-1, 1]$ are unions of periodic orbits. This is shown in Figure A.4, which compares the numerical phase lines of the system (A.1) and level sets of the function (A.7). There is no need to appeal to, say, the Poincaré-Bendixson Theorem [38] here, as all of the information about the orbits (not just their convergence in the limit) may be read from V.

The full system (4.31) contains linear combinations of vertices, which beget more complex dynamics, however we can apply conclusions from the $n = 1$ system

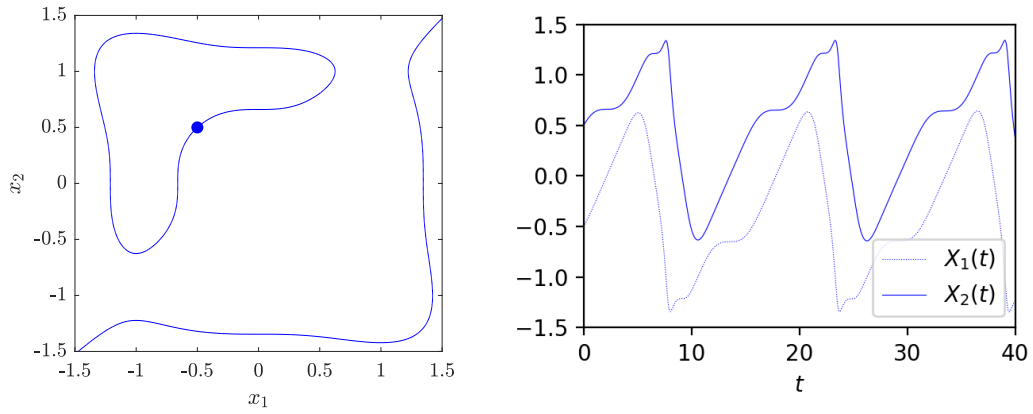

Figure A.4: Periodic dynamics for $\alpha = 1$. Plot of the level set of $V(x_1, x_2)$ containing $(-0.5, 0.5)$ (left), and the associated dynamics of the full system (4.31) with initial conditions $X_1(0) = -0.5\,\mathbf{1}_{n\times n}$ and $X_2(0) = 0.5\,\mathbf{1}_{n\times n}$ (right).

to the full system in the case of the initial conditions $X_1(0) = x_{0(1)}\,\mathbf{1}_{n\times n}$ and $X_2(0) = x_{0(2)}\,\mathbf{1}_{n\times n}$. Given $R = 1$, the only difference is that the full system dynamics move faster by a factor of n, but the orbits are identical, as shown in Figure A.4.

A.3 First integral for $\alpha = 0$

We apply the same approach for $\alpha = 0$, yielding the first integral

$$V(x_1, x_2) = x_1^{-1} - x_2^{-1} + \frac{1}{2}\log\left(\frac{|x_2+1||1-x_1|}{|1-x_2||x_1+1|}\right), \quad x_1, x_2 \notin \{-1, 0, 1\}, \quad \text{(A.8)}$$

for which the level sets are plotted alongside the numerical phase portrait in Figure A.5. Note also that the lines $x_1 = \gamma$ and $x_2 = \gamma$ are invariant sets for $\gamma \in \{-1, 0, 1\}$. Orbits in the domain Ω which do not start on these lines tend towards the top-right fixed point of the quadrant in which they begin.

For $\alpha = 1/2$, the first integral is given by $x_1 - x_2 = c$, for some constant c, which can be observed from Figure A.1.

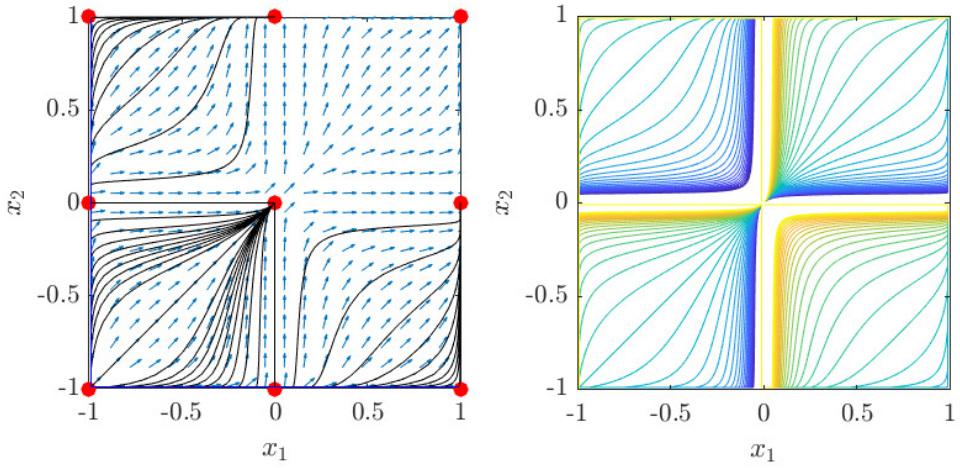

Figure A.5: Numerical phase portrait of the system (A.3) with $\alpha = 0$ (left). The black phase lines are initialised just inside the domain of interest along the lines $L_1 := (-0.99, t)$ and $L_2 := (t, -0.99)$ for $t \in [-0.99, 0.99]$. The right plot shows level sets of the function (A.8).

A.4 Regions of convergence

A necessary condition for the $\alpha = 0$ orbits inside Ω, shown in Figure A.5, is that the set of fixed points in the first quadrant $\mathcal{Q}_1 = \{(0,0), (0,1), (1,0), (1,1)\}$ is an asymptotic set for orbits beginning in any region $S \subset \Omega$. This applies in general for $0 \leq \alpha < 1/2$, where Figure A.6 plots each orbit associated to its ω-limit point by colour. It is worth noting from Figure A.6 that there exists a region $\mathcal{G}$ in the third quadrant from which orbits will tend towards $(1,1)$, plotted in green. The size of this region increases from zero with $0 \leq \alpha < 1/2$. We view this behaviour as a limitation of the model when applied to multiplex social networks. The reason is that we are associating two coupled layers of constant negative relations, and have both graphs tend to consensus states, which does not seem realistic. It is in fact observed for some non-constant matrices with normally distributed negative initial conditions. If two matrices are drawn from normal distributions with means $\mu_1, \mu_2 < 0$, in the decoupled state, both layers tend to a bipolar state, but when coupled they may both tend to consensus, as in Figure A.7.

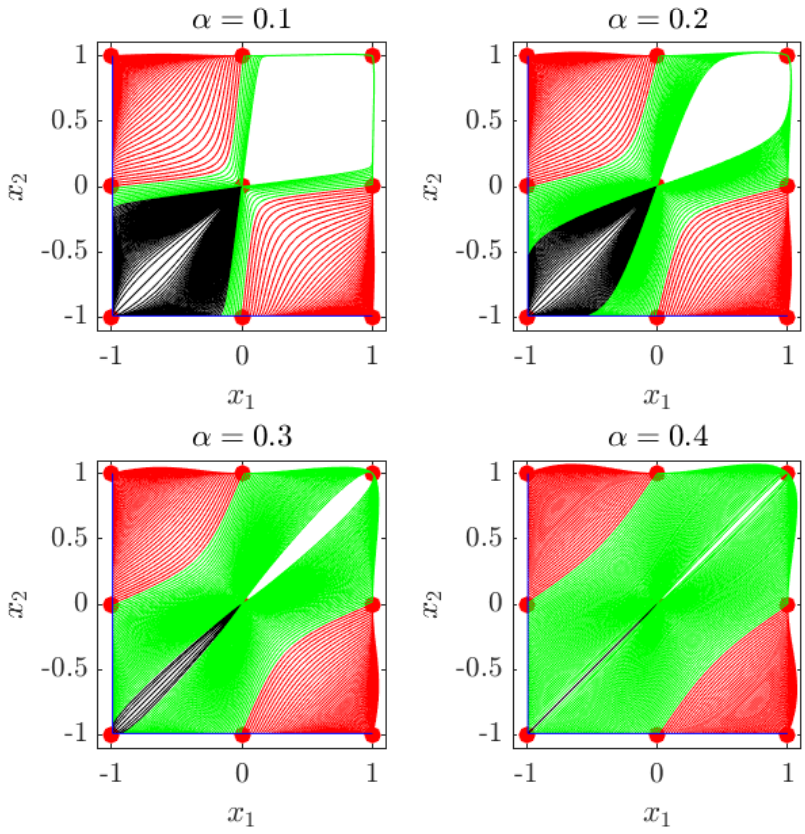

Figure A.6: Orbits beginning in the region $S \subset \Omega$, each associated to its ω-limit point by colour: red for $(0,1)$, $(1,0)$, green for $(1,1)$, and black for $(0,0)$. Note the small overshoot of the fixed point for larger values of α, indicating oscillatory behaviour.

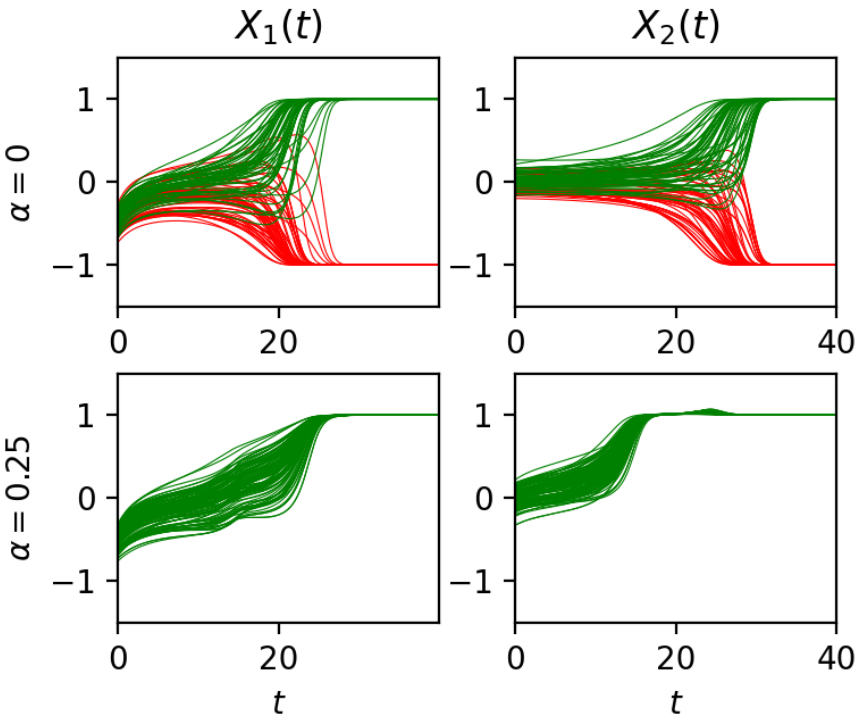

Figure A.7: Multiplex dynamics with initial conditions drawn from a normal distribution with $\mu_1 = -0.5$ and $\mu = 0$ for $X_1(0)$ and $X_2(0)$ respectively. Independently, both layers tend to bipolar states of balance (top row), but when coupled, both tend to consensus. The small overshoot of the fixed point in the bottom right replicates similar behaviour of the $n = 1$ trajectories in Figure A.6.

Appendix B

Local stability of multiplex fixed points for $n = 1$

Figures B.1 and B.2 on the following pages are results of the numerical study of the local stability of fixed points in the multiplex system (A.3).

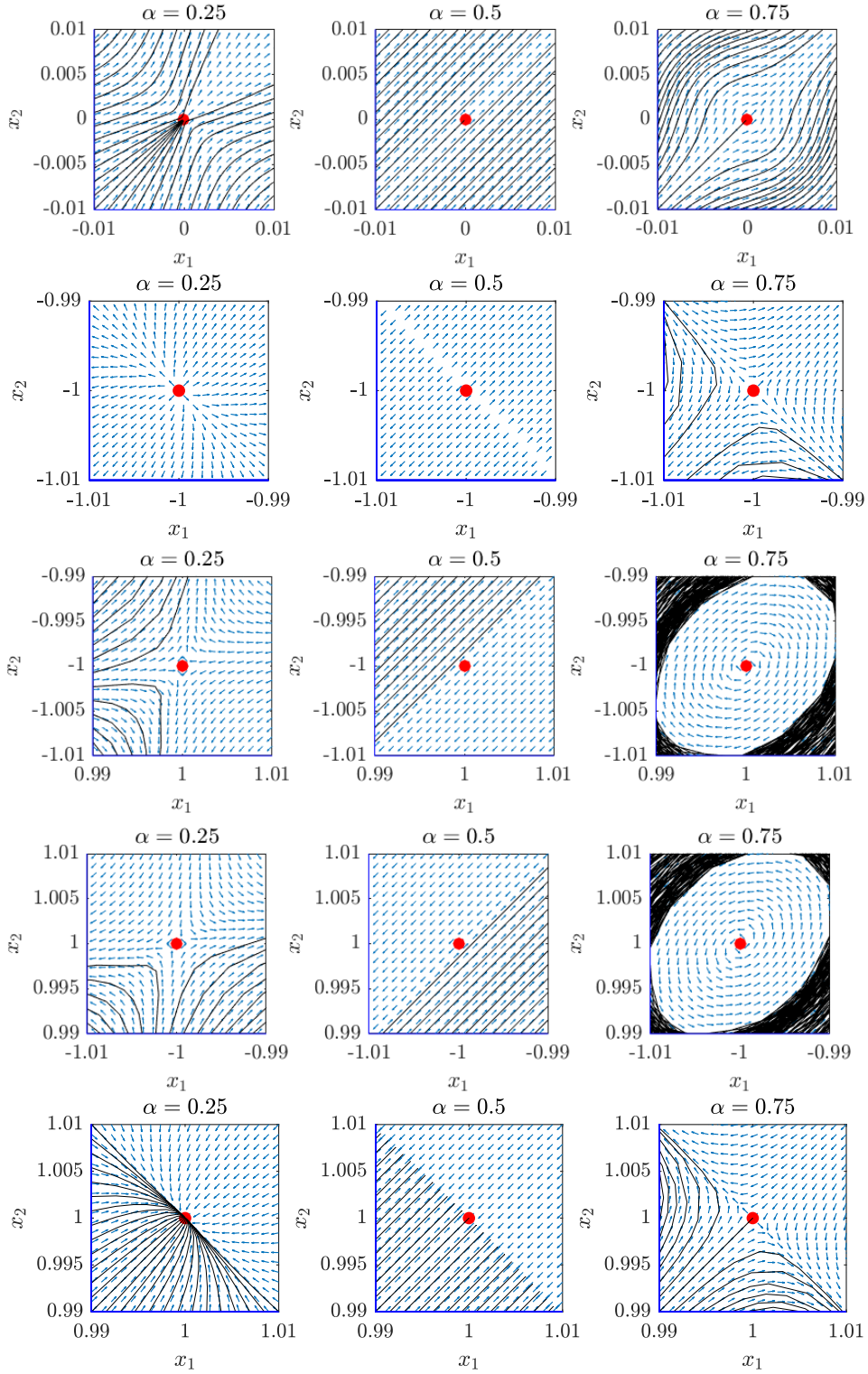

Figure B.1: Local phase plots around origin and corner fixed points.

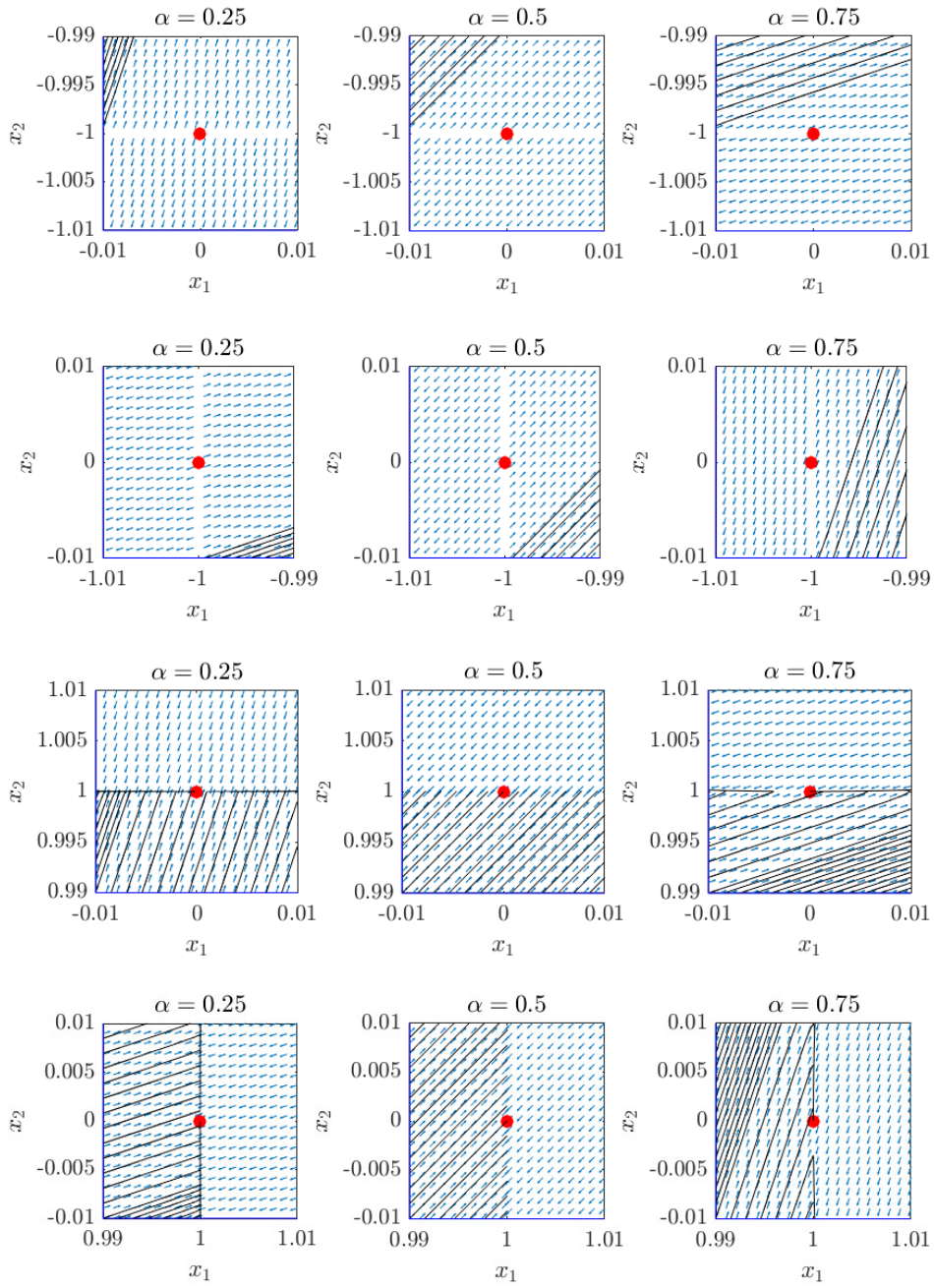

Figure B.2: Local phase plots around other fixed points.

Bibliography

[1] D. Cartwright and F. Harary. Structural balance: a generalization of Heider's theory. *Psychological review*, 63(5):277–293, 1956.

[2] L. F. Richardson. Frequency of occurrence of wars and other fatal quarrels. *Nature*, 148(3759):598–598, 1941.

[3] H. Mueller and C. Rauh. Reading between the lines: Prediction of political violence using newspaper text. *American Political Science Review*, 112(2):358–375, 2018.

[4] S. Tench, H. Fry, and P. Gill. Spatio-temporal patterns of IED usage by the Provisional Irish Republican Army. *European Journal of Applied Mathematics*, 27(3):377–402, 2016.

[5] V. Cervantes. *The Complex System of International Relations*. PhD thesis, Mathematics Department, University of Namur, 2020.

[6] R. A. Hegemann, L. M. Smith, A. B. T. Barbaro, A. L. Bertozzi, S. E. Reid, and G. E. Tita. Geographical influences of an emerging network of gang rivalries. *Physica A: Statistical Mechanics and its Applications*, 390(21):3894–3914, 2011.

[7] M. Lim, R. Metzler, and Y. Bar-Yam. Global pattern formation and ethnic/cultural violence. *Science*, 317(5844):1540–1544, 2007.

[8] P. Turchin, T. E. Currie, E. A. Turner, and S. Gavrilets. War, space, and the evolution of Old World complex societies. *Proceedings of the National Academy of Sciences*, 110(41):16384–16389, 2013.

[9] J. D. Botero, W. Guo, G. Mosquera, A. Wilson, S. Johnson, G. A. Aguirre-Garcia, and L. A. Pachon. Gang confrontation: the case of Medellin (Colombia). *PloS one*, 14(12):e0225689, 2019.

[10] M. E. J. Newman. *Networks : an introduction*. Oxford University Press, Oxford, 2010.

[11] L. Pan, H. Shao, M. Mesbahi, D. Li, and Y. Xi. Structural balance of multiplex signed networks: A distributed data-driven approach. *Physica A: Statistical Mechanics and its Applications*, 508:748–756, 2018.

[12] B. A. Cipra. An introduction to the Ising model. *The American Mathematical Monthly*, 94(10):937–959, 1987.

[13] F. Heider. Attitudes and cognitive organization. *The Journal of psychology*, 21(1):107–112, 1946.

[14] T. M. Newcomb. An approach to the study of communicative acts. *Psychological review*, 60(6):393, 1953.

[15] F. Harary. On the notion of balance of a signed graph. *Michigan Mathematical Journal*, 2(2):143–146, 1953.

[16] E. Terzi and M. Winkler. A spectral algorithm for computing social balance. In *International Workshop on Algorithms and Models for the Web-Graph*, pages 1–13. Springer, 2011.

[17] K. Kułakowski, P. Gawroński, and P. Gronek. The Heider balance: A continuous approach. *International Journal of Modern Physics C*, 16(05):707–716, 2005.

[18] J. E. Rauch and A. Casella. *Networks and markets*. Russell Sage Foundation, 2001.

[19] S. A. Marvel, J. Kleinberg, R. D. Kleinberg, and S. H. Strogatz. Continuous-time model of structural balance. *Proceedings of the National Academy of Sciences*, 108(5):1771–1776, 2011.

[20] V. A. Traag, P. Van Dooren, and P. De Leenheer. Dynamical models explaining social balance and evolution of cooperation. *PloS one*, 8(4):e60063, 2013.

[21] X. Zheng, D. Zeng, and F. Y. Wang. Social balance in signed networks. *Information Systems Frontiers*, 17(5):1077–1095, 2015.

[22] N. P. Hummon and P. Doreian. Some dynamics of social balance processes: bringing Heider back into balance theory. *Social Networks*, 25(1):17–49, 2003.

[23] L. E. Cederman and N. B. Weidmann. Predicting armed conflict: Time to adjust our expectations? *Science*, 355(6324):474–476, 2017.

[24] T. Antal, P. L. Krapivsky, and S. Redner. Social balance on networks: The dynamics of friendship and enmity. *Physica D: Nonlinear Phenomena*, 224(1):130–136, 2006.

[25] M. Moore. Structural balance and international relations. *European Journal of Social Psychology*, 1979.

[26] R. Smeets, M. De Pourcq, and A. van den Bosch. Modeling conflict: Representations of social groups in present-day Dutch literature. *Journal of Cultural Analytics*, page 24722, 2021.

[27] M. Szell, R. Lambiotte, and S. Thurner. Multirelational organization of large-scale social networks in an online world. 107(31):13636–13641, 2010.

[28] E. S. Bogardus. Measuring social distance. *Journal of applied sociology*, 9:299–308, 1925.

[29] S. Wongkaew, M. Caponigro, K. Kułakowski, and A. Borzì. On the control of the Heider balance model. *The European Physical Journal Special Topics*, 224(17):3325–3342, 2015.

[30] L. Arnold. On Wigner's semicircle law for the eigenvalues of random matrices. *Zeitschrift für Wahrscheinlichkeitstheorie und verwandte Gebiete*, 19(3):191–198, 1971.

[31] R. Tagiuri, R. Blake, and J. S. Bruner. Some determinants of the perception of positive and negative feelings in others. *The Journal of Abnormal and Social Psychology*, 48(4):585, 1953.

[32] Y. Shang. On the structural balance dynamics under perceived sentiment. *Bulletin of the Iranian Mathematical Society*, 46(3):717–724, 2020.

[33] Z. Bai and Y. Yin. Necessary and sufficient conditions for almost sure convergence of the largest eigenvalue of a Wigner matrix. *The Annals of Probability*, pages 1729–1741, 1988.

[34] W. W. Zachary. An information flow model for conflict and fission in small groups. *Journal of anthropological research*, 33(4):452–473, 1977.

[35] F. Zhang. *The Schur complement and its applications*, volume 4. Springer Science & Business Media, 2006.

[36] M. Medo, M. Mariani, and L. Lü. The fragility of opinion formation in a complex world. *Communications Physics*, 4(1):1–10, 2021.

[37] J. A. Davis. Clustering and structural balance in graphs. *Human Relations*, 20(2):181–187, 1967.

[38] L. Perko. *Differential equations and dynamical systems*, volume 7. Springer Science & Business Media, 2013.

[39] S. J. Chapman. Lecture notes in *B5.6 Nonlinear systems*. Mathematical Institute, University of Oxford, URL: https://courses-archive.maths.ox.ac.uk/node/view_material/53759 (accessed 2/8/21), 2021.

[40] H. R. Dullin and A. V. Ivanov. Another look at the saddle-centre bifurcation: Vanishing twist. *Physica D: Nonlinear Phenomena*, 211(1-2):47–56, 2005.

[41] J. Guckenheimer and P. Holmes. *Nonlinear oscillations, dynamical systems, and bifurcations of vector fields*, volume 42. Springer Science & Business Media, 2013.